Impacts of Atmospheric Nitrogen Deposition on Surface Waters of the Western North Atlantic Mitigated by Multiple Feedbacks

P. St-Laurent[1], M.A.M. Friedrichs[1], R.G. Najjar[2], D.K. Martins[3], M. Herrmann[2], S.K. Miller[2]and J. Wilkin[4]

[1]Virginia Institute of Marine Science, College of William & Mary, Gloucester Point, VA
[2]Department of Meteorology and Atmospheric Science, The Pennsylvania State University, University Park, PA
[3]FLIR Systems, Inc., 3000 Kent Avenue, West Lafayette, IN
[4]Department of Marine and Coastal Sciences, Rutgers University, New Brunswick, NJ

Key Points:

- Air quality model simulations reveal hot-spot of atmospheric nitrogen deposition over Gulf Stream (35–40°N)
- Impact of atmospheric nitrogen deposition on ocean primary productivity is mitigated by multiple feedback processes
- Atmospheric deposition increases new primary production by 22% during summer (8% on average over the year) in Gulf Stream region

Corresponding author: Pierre St-Laurent, `pst-laurent@vims.edu`

Abstract

The impacts of Atmospheric Nitrogen Deposition (AND) on the chlorophyll and nitrogen dynamics of surface waters in the western North Atlantic (25–45°N, 65–80°W) are examined with a biogeochemical ocean model forced with a regional atmospheric chemistry model (Community Multi-scale Air Quality model, CMAQ). CMAQ simulations with year-specific emissions reveal the existence of a 'hot-spot' of AND over the Gulf Stream. The impact of the hot-spot on the oceanic biogeochemistry is mitigated in three ways by physical and biogeochemical processes. First, AND significantly contributes to surface oceanic nitrogen concentrations only during the summer period, when the stratification is maximal and the background nitrogen inventories are minimal. Second, the increase in summer surface nitrate concentrations is accompanied by a reduction in upward nitrate diffusion at the base of the surface layer. This negative feedback partly cancels the nitrogen enrichment from AND. Third, gains in biomass near the surface force a shoaling of the euphotic layer and a reduction of about 5% in deep primary production and biomass on the continental shelf. Despite these mitigating processes, the impacts of AND remain substantial. AND increases surface nitrate concentrations in the Gulf Stream region by 14% during the summer (2% on average over the year). New primary production increases by 22% in this region during summer (8% on average). Although these changes may be difficult to distinguish from natural variability in observations, the results support the view that AND significantly enhances local carbon export.

1 Introduction

The surface of the global ocean warmed by $\sim$ 0.11°C per decade between 1971 and 2010, resulting in a 4% increase in thermal stratification [*Rhein et al.*, 2013]. This increased stratification implies a decrease in surface nutrients and primary production in the vast portions of the ocean where the nutrient supply depends on vertical mixing [e.g., *Behrenfeld et al.*, 2006]. *Wang et al.* [2015] recently suggested that this trend could be mitigated by anthropogenic aerosol deposition, a process where nutrients resulting from human activities fertilize the upper ocean. An increasing number of studies are examining this process in different regions of the ocean [e.g., *Doney et al.*, 2007]. In the North Pacific Ocean, *Kim et al.* [2011] report that Atmospheric Nitrogen Deposition (AND) coupled with increased riverine inputs forced a switch in the primary production from being nitrogen-limited to being phosphorus-limited. The increase in atmospheric deposition was due to anthropogenic activity and was concentrated near the Asian continent [*Kim et al.*, 2014a].

The waters of the northeastern United States (US) represent another region where AND is expected to have a measurable effect on primary production. This area is positioned downwind of highly urbanized areas, agricultural centers and industrial centers including coal-fired power plants (see the airsheds in *Paerl et al.* [2002]). All these sources contribute to atmospheric nitrogen concentrations in oxidized or reduced forms [*Linker et al.*, 2013; *Li et al.*, 2016]. Moreover, the waters offshelf are oligotrophic during the summer with surface nitrate (NO_3^-) concentrations as low as 0.2 mmol-N m^{-3} [*Boyer et al.*, 2013]. The nitrogen-limited surface layer is thus expected to respond to AND events. For example, bioassays conducted in the Gulf Stream and Sargasso Sea showed stimulated CO_2 fixation in response to natural rainfall [*Paerl et al.*, 1999]. AND is estimated to represent 24% of the new nitrogen inputs in surface waters of the Sargasso Sea [*Paerl*, 1995]. The contribution from organic nitrogen remains uncertain but *Peierls and Paerl* [1997] estimate that 20–30% of the organic N deposited would be available to primary producers.

Kim et al. [2014b] examined the effect of AND in this area by comparing satellite-derived surface chlorophyll to atmospheric conditions. The results show that precipitation events in low-nitrate areas ($<$ 1 mmol-N m^{-3}) are associated with increased chlorophyll while high-nitrate areas often exhibit a decrease in chlorophyll during such events. The

authors suggest that the strong winds accompanying precipitation events would reduce light availability by mixing phytoplankton deeper into the water column and thus overcome the beneficial effect of AND where NO_3^- is already abundant. However, the limited data available made it difficult to disentangle such physical effects from the direct biogeochemical effects of AND.

Here we present results from the Deposition of Atmospheric Nitrogen to Coastal Ecosystems (DANCE) project, whose aim is to assess the impact of AND on surface waters of the western North Atlantic. A central hypothesis of DANCE is that precipitation events elevate primary production and phytoplankton biomass in these waters during the summer, when oligotrophic and stratified conditions prevail. Our goal here is to evaluate the role of AND in the western North Atlantic over several years. We employ numerical simulations for the period 2004–2008 at high spatial ($\sim$ 9 km) and temporal (3-hourly atmospheric forcing) resolution. The model framework combines deposition rates from an atmospheric chemistry model with a 3-D oceanic model (Figure 1) that includes an ecological module for the lower trophic levels [*Hofmann et al.*, 2011; *Druon et al.*, 2010; *Cahill et al.*, 2016]. The numerical experiments allow us to isolate the impact of AND from other physical processes such as wind mixing that often co-occur with precipitation events. Though the impact of AND on marine biogeochemistry has been modeled in the past, the focus has been primarily at the global scale using coarse-resolution models [horizontal scale $\sim$ 200 km; *Duce et al.*, 2008; *Krishnamurthy et al.*, 2007]. However, AND is highly localized in coastal waters downwind of industrialized regions [e.g., *Martins et al.*, 2016]. Furthermore, coastal ocean physical and biogeochemical dynamics are characterized by high spatial variability, on the order of tens of km. This study therefore addresses the need to model the impacts of AND on the western North Atlantic at the appropriate spatial scale.

The next section describes the model framework, the datasets used and the numerical experiments conducted. The following sections examine the variability of AND events, the surface NO_3^- budget in the presence/absence of AND, and the effect of AND on the primary production of the system. A discussion of the results and their relevance in the context of the carbon cycle conclude this study.

2 Method

2.1 Atmospheric nitrogen deposition forcing

The atmospheric nitrogen deposition estimates used in the present study were simulated by the US Environmental Protection Agency (EPA) Atmospheric Science Modeling Division using the Community Multi-scale Air Quality model [CMAQ version 5.0.2, *Appel et al.*, 2013; *Gantt et al.*, 2015]. CMAQ is an open-source (https://www.epa.gov/cmaq) air quality modeling system that links together models of atmospheric chemistry, transport, meteorology, and emission to predict fate and transport of a broad spectrum of atmospheric constituents. The model notably calculates the concentration of ions in rain at regular interval over the course of a precipitation event and thus represents processes such as the washout effect. We obtained from the EPA the archived monthly averaged outputs of atmospheric deposition at the surface for all nitrogen species simulated by CMAQ. This output is from the current regional EPA configuration of the model, with year-specific emissions, meteorological simulations using the WRF 3.4 [Weather Research and Forecasting, *Skamarock et al.*, 2008] meteorological model, and CB05TUCL chemical mechanisms [*Sarwar et al.*, 2011], set up at 12 km horizontal resolution and 35 vertical layers. CMAQ nitrogen species were aggregated into wet and dry deposition and, within each deposition type, further aggregated into reduced (NH_3 and NH_4^+) and oxidized (HNO_3, NO_3^-, NO, NO_2, N_2O_5, HNO_2, organic nitrate, peroxyacetyl nitrate and higher peroxyacyl nitrates) species to respectively match the ammonium and nitrate pools of the ocean model (see Section 2.3).

The archived monthly outputs from CMAQ represent long-term averages of individual events localized in space and time (duration is O(day) or less for precipitation events). Some form of temporal downscaling is thus required to simulate the biological response to individual events. This is particularly important for wet deposition events whose variability follows that of rain events. The downscaling approach used in this study is to: (1) derive monthly rain concentration fields from CMAQ's archived monthly wet deposition and rain fields, and (2) multiply these concentrations by 3-hourly precipitation fields [*Huffman et al.*, 2007, see below] to yield a 3-hourly flux at the ocean surface. The result of this downscaling approach is a 3-hourly wet deposition that reproduces the episodic nature and patchiness of precipitation.

In the first step of the downscaling approach, the concentration fields are calculated as:

$$\begin{aligned} OXI_{\text{rain}} &= \frac{WD^{\text{oxidized}}_{\text{cmaq}}}{\text{rain}_{\text{cmaq}}}, \\ RED_{\text{rain}} &= \frac{WD^{\text{reduced}}_{\text{cmaq}}}{\text{rain}_{\text{cmaq}}}, \end{aligned} \tag{1}$$

where OXI_{rain} is the monthly rain concentration field for oxidized nitrogen, $WD^{\text{oxidized}}_{\text{cmaq}}$ is the monthly wet deposition flux of oxidized nitrogen, and $\text{rain}_{\text{cmaq}}$ is the monthly precipitation rate from CMAQ (and so on for reduced nitrogen). In the second step, the downscaled wet nitrogen fluxes are calculated as:

$$\begin{aligned} WD^{\text{oxidized}} &= OXI_{\text{rain}} \times \text{rain}_{3\,\text{hourly}}, \\ WD^{\text{reduced}} &= RED_{\text{rain}} \times \text{rain}_{3\,\text{hourly}}, \end{aligned} \tag{2}$$

where $\text{rain}_{3\,\text{hourly}}$ is a 3-hourly precipitation field. A comparison between four precipitation products [*Dee et al.*, 2011; *Mesinger et al.*, 2006; *Huffman et al.*, 2007; *Appel et al.*, 2013] showed similar rates over the US mainland but major differences over the Gulf Stream region. Given the importance of precipitation in this study, we use 3-hourly, 0.25°-resolution fields from the Tropical Rainfall Measuring Mission [TRMM, *Huffman et al.*, 2007]. This product has been extensively compared against observations and is expected to be the most accurate of the four over the open ocean.

Version 5.0.2 of CMAQ does not include the bulk of dissolved organic nitrogen (DON) in rainwater even though DON contributes significantly to AND [*Cornell et al.*, 2003; *Zhang et al.*, 2012; *Jickells et al.*, 2013]. Wet deposition of DON is thus estimated following Zhang et al. (2012, their Figure 5c). This parameterization assumes DON concentrations in rain to be proportional to total dissolved nitrogen (the sum of oxidized nitrogen, reduced nitrogen and DON):

$$\text{DON}_{\text{rain}} \approx 0.24 \times (OXI_{\text{rain}} + RED_{\text{rain}} + \text{DON}_{\text{rain}}), \tag{3}$$

which can be solved for DON_{rain}. Note that the regression of Zhang et al. (2012) has a non-zero intercept ($4.57\,\mu\text{mol L}^{-1}$). This intercept has a very small effect on the final values and has no physical meaning (DON must be zero when total dissolved nitrogen is zero). We therefore neglect the intercept altogether. The downscaled wet DON flux is calculated from DON_{rain} as in Eqs. 2.

A drawback of the downscaling procedure (Eqs. 1,2) is that the resulting wet deposition rates are not exactly the same as in the original CMAQ outputs because CMAQ precipitation differs from TRMM precipitation. To evaluate the magnitude of this error, we conducted identical numerical experiments with the archived CMAQ wet deposition fields and the downscaled wet deposition fields. The changes in biological fields caused by AND in the two runs were typically indistinguishable. This indicates that the bias incurred by the downscaling procedure is minor. Another drawback of using CMAQ's monthly averaged rain concentration fields (Eq. 1) is that the concentration is mostly constant during

a single precipitation event. This means that high-precipitation events may have too much N and low-precipitation events may have too little N.

For dry nitrogen deposition, CMAQ provides monthly deposition fields of oxidized and reduced nitrogen. No temporal downscaling is applied to these fields as dry deposition is assumed to vary over longer temporal scales than wet deposition. Dry deposition of DON is neglected altogether since no data are available. Note that the CMAQ domain does not cover the entire oceanic domain (Figure 1). The CMAQ fields were thus extrapolated over the missing regions using a nearest-neighbor approach. The analyses of the present study are limited to regions contained within the original CMAQ domain.

AND is introduced in the ocean model as a 3-hourly flux of nitrogen at the ocean surface (see Section 2.3). The fluxes of oxidized and reduced nitrogen are added to the oceanic nitrate and ammonium pools, respectively, while the flux of DON is added to the semilabile fraction of oceanic DON. For experiments including both wet and dry nitrogen deposition, the monthly dry AND fields from CMAQ are temporally interpolated over the same 3-hourly time-axis as the wet fluxes and then combined with the wet fluxes (see Section 2.4).

2.2 Atmospheric data used for the evaluation of CMAQ

CMAQ has been extensively used to study air quality and atmospheric deposition in the US, with several studies focused on its simulation of AND and related quantities, such as ammonia, nitrate, and NO_2 concentrations. *Appel et al.* [2011] found that the wet deposition simulated by an earlier version of CMAQ (version 4.7) over the eastern two thirds of the US is, on average, too low for NH_4^+ in all seasons and for NO_3^- in the spring and summer. Shortcomings of the ammonia simulation in this model version appear to be related to CMAQ's meteorology, NH_3 lifetime, and NH_3 emissions [*Eder et al.*, 2014]. Indeed, modifications by *Bash et al.* [2013], which coupled a photochemical air-quality model with an agroecosystem model in CMAQ version 5.0 to simulate the bidirectional exchange of NH_3, resulted in improved simulations of NH_4^+ wet deposition and nitrate aerosol concentrations. *Canty et al.* [2015] found that version 4.7's simulation of the vertical column NO_2, which is expected to be related to nitrogen deposition, is too high in urban areas and too low in rural areas of the northeastern US. Finally, *Gantt et al.* [2015] evaluated CMAQ version 5.02's ability to simulate surface nitrate concentrations near Tampa Bay, Florida and found improvements due to inclusion of sea spray aerosols. This version (5.02) is the one used in the present study.

Despite the fairly extensive evaluation of CMAQ AND and related quantities, we are not aware of a detailed evaluation of any model version of CMAQ based on the deposition of nitrate and ammonia along the US east coast, particularly during summer, which is when, we hypothesize, that the impacts of nitrogen deposition will be greatest on ocean biogeochemistry. We thus conducted an evaluation of CMAQ wet deposition of nitrate and ammonia (see Section 3) at the 25 National Trends Network (NTN) stations that were within 50 km of the coast between 2004 and 2008 (Figure 1); we are unaware of any N deposition measurement inside the ocean model domain. The NTN deposition rates are based on weekly measurements of precipitation and concentrations of NH_4^+ and NO_3^- made as part of the National Atmospheric Deposition Program (http://nadp.sws.uiuc.edu/NTN/ntnData.aspx). We did not include dry deposition in the model evaluation because observed estimates of dry deposition are model dependent [*Meyers et al.*, 1998; *Schwede and Lear*, 2014].

2.3 3-D oceanic model

The oceanic model is an application of the Regional Ocean Modeling System [ROMS, *Shchepetkin and McWilliams*, 2005] for the North-Eastern North American (NENA) domain [Figure 1; *Fennel et al.*, 2006, 2008; *Hofmann et al.*, 2008]. The model has a quasi-

uniform horizontal resolution of 9 km with 30 topography-following vertical levels. The thickness of the uppermost vertical level varies from a few centimeters in shallow water to 13 m at the deepest point of the model domain. The model is forced at its oceanic boundaries with outputs from the Navy Coupled Oceanic Data Assimilation reanalysis [NCODA, *Cummings*, 2005]. In addition, five tidal constituents from the model of *Egbert and Erofeeva* [2002] are prescribed at the oceanic boundaries (O1, K1, N2, M2 and S2). The model domain includes 31 rivers positioned from Florida to Nova Scotia that provide realistic fluxes of momentum, freshwater, temperature and the 19 state variables of the biogeochemical module (described below).

Atmospheric conditions at the ocean surface are obtained from the North-American Regional Reanalysis [NARR, *Mesinger et al.*, 2006] except precipitation (see Section 2.1). Surface fluxes are calculated from the atmospheric and oceanic surface fields using the algorithms of *Fairall et al.* [2003]. The initial model condition (Nov. 5, 2003), the boundary conditions and the spin-up procedure are described in detail in *Hofmann et al.* [2011]. The ocean model is integrated in time from Nov. 5, 2003 to Dec. 31, 2008 with relaxation to the NCODA fields along the perimeter of the domain (nudging zones; see Figure 1). Physical and biological scalar fields are advected with a sign-preserving 3-D advection scheme [*Smolarkiewicz and Margolin*, 1998]. Sub-grid scale vertical viscosity and diffusivity are parameterized with the level-2.5 model of *Mellor and Yamada* [1982].

The physical ocean model is coupled to a biogeochemical module representing the lower trophic levels. This module was extended from *Druon et al.* [2010], *Hofmann et al.* [2011] and *Cahill et al.* [2016] to include two size classes of plankton and better represent the surface chlorophyll fields. These modifications were based on the optimal model complexity study of *Xiao and Friedrichs* [2014a]. Parameter values for the additional plankton size class formulations were obtained via variational adjoint parameter optimization analyses [*Xiao and Friedrichs*, 2014b]. The version used in the present study has 19 state variables: NO_3^-, NH_4^+, oxygen, total inorganic carbon, alkalinity, small/large phytoplankton, small/large chlorophyll, small/large zooplankton, small/large nitrogen/carbon from detritus, and semilabile/refractory dissolved organic nitrogen/carbon. The model neglects the phytoplankton growth limitation by phosphorus availability and this simplification is discussed in Section 6. The Supporting Information includes a model-data comparison for nitrate and chlorophyll and a list of the model equations and parameters.

2.4 Numerical experiments conducted

We examine the effects of AND by conducting three different numerical experiments covering the period of Nov. 5, 2003 to Dec. 31, 2008. The first experiment represents a control simulation and does not include AND (Run 1). The second experiment includes both wet and dry AND (Run 2). The third experiment (Run 3) only includes wet AND and allows us to quantify the relative importance of wet and dry deposition. We assume that the effects of dry deposition can be isolated by simple subtraction (i.e., we assume a linear response to AND).

All three numerical experiments are conducted in identical conditions (model parameters, executable, processors) so that the physical fields (salinity, temperature, currents, diffusivity; re-calculated in each experiment) are bit-for-bit identical. The differences in the biological fields are thus solely due to the presence/absence of AND. This approach allows us to isolate the impact of AND from other processes such as vertical mixing during precipitation events [see *Kim et al.*, 2014b].

We conduct our analyses of the biological response to AND in three regions of the model domain: the Gulf Stream region (GS), the Sub-Tropical Gyre (STG), and the continental shelf of the Mid-Atlantic Bight (MAB; see Figure 1). These three regions were chosen because they are located within the original CMAQ domain and represent different regimes: low nitrogen inventory and high deposition (GS), low nitrogen inventory and

low deposition (STG), and high nitrogen inventory and moderate deposition (MAB). We purposely exclude coastal systems such as estuaries and embayments from the regions analyzed. These regions of high nitrate concentrations are less likely to respond to AND and they are not well represented by the model mesh size (9 km).

3 Evaluation of CMAQ

The CMAQ-simulated wet deposition of NO_3^- + HNO_3 and NH_4^+ + NH_3 are compared to observed wet deposition of NO_3^- and NH_4^+ (respectively) in Figure 2. Overall, CMAQ is found to simulate AND quite well along the US east coast. There are slight overall biases, with the annual mean CMAQ NO_3^- + HNO_3 and NH_4^+ + NH_3 wet deposition rates at the NTN sites differing from observed NO_3^- and NH_4^+ by −9% and −2%, respectively. Summertime simulations are less skillful, with biases in NO_3^- + HNO_3 and NH_4^+ + NH_3 deposition of −14% and +36%, respectively. The NH_4^+ + NH_3 overestimation stems from fairly large differences south of 35°N. However, the summer errors are compensating such that the overall bias in wet deposition of inorganic nitrogen (NO_3^- + HNO_3 + NH_4^+ + NH_3) is only 7% above observed NO_3^- + NH_4^+. Finally, CMAQ captures the latitudinal pattern in the deposition rates, which show maxima at about 35°N in annual and summer NH_4^+ deposition and somewhat weaker maxima for annual NO_3^- deposition at 40°N.

4 Theory: Nitrogen enrichment and modeled biological response

To facilitate the interpretation of the results, we now discuss the factors regulating primary production in the ocean model. The biogeochemical module includes two pools of dissolved inorganic nitrogen (NO_3^- and NH_4^+) and two size classes of phytoplankton: small phytoplankton (*SP*) and large phytoplankton (*LP*). Primary production (*PP*) is the resultant of four contributions:

$$\begin{aligned} PP &= \mu_{SP} L_I^{SP} L_{\mathrm{NO3}}^{SP} SP + \mu_{LP} L_I^{LP} L_{\mathrm{NO3}}^{LP} LP \\ &+ \mu_{SP} L_I^{SP} L_{\mathrm{NH4}}^{SP} SP + \mu_{LP} L_I^{LP} L_{\mathrm{NH4}}^{LP} LP \\ &= PP^{\mathrm{NO3}} + PP^{\mathrm{NH4}}, \end{aligned} \tag{4}$$

where the upper line of Eq. 4 represents the contribution from NO_3^- uptake (PP^{NO3}) and the lower line the NH_4^+ uptake (PP^{NH4}). μ is the growth rate, L_I is the limitation from light and the nutrient limitation is formulated as:

$$L_{\mathrm{NO3}} = \frac{\mathrm{NO3}}{\mathrm{NO3} + K_{\mathrm{NO3}}} \frac{1}{1 + \mathrm{NH4}/K_{\mathrm{NH4}}}, \quad L_{\mathrm{NH4}} = \frac{\mathrm{NH4}}{\mathrm{NH4} + K_{\mathrm{NH4}}}, \tag{5}$$

where $K_{\mathrm{NO3}}, K_{\mathrm{NH4}}$ are half-saturation coefficients specific to *SP* and *LP* (see Supporting Information). The model does not include a growth limitation by phosphorus availability and this simplification is discussed in Section 6.

A simple expression for the relative change in *PP* due to AND can be obtained with the following assumptions: the functions μ and L_I are largely unchanged by atmospheric deposition (at least near the surface), the production is dominated by one phytoplankton species (e.g. *SP* in the GS and STG regions), and water column nitrogen concentrations are sufficiently low for the Michaelis-Menten relations (Eq. 5) to be linearized. With these assumptions, the relative increase in NO_3^- uptake reduces to:

$$\frac{PP^{\mathrm{NO3}}_{\text{with deposition}}}{PP^{\mathrm{NO3}}_{\text{no deposition}}} \approx \frac{\mathrm{NO3}_{\text{with deposition}}}{\mathrm{NO3}_{\text{no deposition}}} \frac{SP_{\text{with deposition}}}{SP_{\text{no deposition}}}, \tag{6}$$

with a similar expression for ammonium uptake. The relative increase in primary production is thus linearly proportional to the relative increase of nitrogen and biomass.

In absence of AND, the new surface primary production of the model is equivalent to the nitrate uptake (PP^{NO3}), while the ammonium uptake (PP^{NH4}) represents the regenerated production. In presence of AND, both PP^{NO3} and PP^{NH4} contribute to the new production since all forms of AND (oxidized N, reduced N and DON) are considered 'new' inputs of nitrogen. The relative increase in new primary production due to AND is thus calculated as:

$$\frac{PP_{\text{with deposition}} - PP_{\text{no deposition}}}{PP^{\mathrm{NO3}}_{\text{no deposition}}}. \tag{7}$$

The numerator of Eq. 7 represents the gain in new production due to deposition of atmospheric nitrogen. The denominator of Eq. 7 is the new production in the absence of AND (i.e., the NO_3^- uptake of the control simulation).

5 Results

5.1 Variability of AND in the western North Atlantic

The spatial variability of the wet atmospheric deposition averaged over 2004–2008 is dominated by the presence of a large 'hot-spot' over the Gulf Stream (Figure 3a,b,c). Wet oxidized N deposition reaches values of up to 3 mmol-N m^{-2} $month^{-1}$ in this particular area, comparable to the largest values observed over the mainland (Figure 3a). Wet reduced N and DON deposition exhibit a similar 'hot-spot' but with significantly lower absolute values. This spatial variability is influenced by precipitation events, which are recurrent along the path of the Gulf Stream (Figure 3f; see also *Hobbs* [1987]). The wet deposition rates over the mainland are consistent with similar maps from *Paerl et al.* [2002]. The spatial variability of dry AND shows a qualitatively different distribution (Figure 3d,e). Deposition rates are much lower over the ocean than on land. The contribution of dry reduced N deposition is virtually zero over the Gulf Stream.

The seasonal variability over the Gulf Stream of atmospheric oxidized N deposition is much greater than that of reduced N and DON (Figure 4). Both wet and dry oxidized N deposition exhibit a large seasonal cycle with maximum values during the winter, despite the fact that precipitation shows only a small seasonal cycle (Figure 4a,b). In January the wet (dry) oxidized N deposition is approximately three times (seven times) as high as the deposition of reduced N, whereas oxidized N and reduced N deposition become roughly comparable in magnitude during the summer season. The seasonality of wet DON deposition is essentially a scaled-down version of wet oxidized N deposition as expected from Eq. 3 and the general dominance of oxidized N deposition. The causes of the seasonal variability were not examined as this is beyond the scope of the present study.

5.2 Sources and sinks of NO_3^- in the three regions

The modeling system described above is used to estimate the nitrogen sinks and sources in our three regions of interest (GS, STG and MAB; Figure 1) and to better understand how AND modifies the existing balance. We specifically focus on NO_3^- because of its importance in the total atmospheric flux (Figure 3). The sinks and sources are calculated with daily averaged model outputs and spatially integrated over the upper 15 m of the three regions. This depth is greater than the thickness of the uppermost vertical level at the deepest point of the model domain to properly represent surface deposition in all areas of the model domain. Each budget term is then averaged over the period 2004–2008. The NO_3^- budget is represented as:

$$\frac{\partial}{\partial t}\iiint \mathrm{NO3}\,\mathrm{d}V = \text{advection} + \text{vertical diffusion} + \text{biology} + \text{deposition} + \text{residual}, \tag{8}$$

where the 'residual' represents nitrification (see Supporting Information) and errors due to calculating the terms from time-averaged outputs. Note that the simulations do not include explicit horizontal diffusion.

The Gulf Stream domain (GS, Figure 1) is characterized by strong vertical gradients of NO_3^- and a near-steady balance between vertical diffusion and NO_3^- uptake (Table 1, Run 1). Horizontal advection is a small sink partly counter-balanced by vertical advection acting as a source of NO_3^-. The last term (residual) is fairly small (its magnitude is only $\sim 6\%$ of the NO_3^- uptake) and has no apparent seasonality (not shown).

The addition of wet and dry deposition represents an extra NO_3^- input (1.46×10^{-6} mmol-N m^{-2} s^{-1}) that amounts to $\sim 10\%$ of the mean NO_3^- uptake in the GS (Table 1, Run 2). Deposition produces a significant increase in surface NO_3^- concentrations during the summer (when the background concentrations are lowest and sensitive to small changes, Section 5.3) and thus contributes to reducing the vertical gradients of NO_3^- in the upper 20 m. As a result, the NO_3^- input from deposition is mitigated by a 0.74×10^{-6} mmol-N m^{-2} s^{-1} reduction in vertical diffusion resulting from these weaker vertical gradients. The net effect of these two tendencies is a 0.64×10^{-6} mmol-N m^{-2} s^{-1} increase in NO_3^- uptake. In other words, 44% of the deposited NO_3^- is converted into extra production while the remainder mostly compensates for the reduction in upward vertical diffusion. The other terms of the budget (advection and temporal derivative) are not significantly affected by the deposition. The lack of change in the other terms suggests a rapid (intra-seasonal) and local utilization of the deposited NO_3^- with no long-term storage.

The offshore oligotrophic STG region is characterized by considerably lower rates of NO_3^- uptake and vertical diffusion (Table 1, Run 1). The balance between the terms is similar to the GS region with uptake and diffusion dominating the budget. Atmospheric deposition is about a third of that in the GS region and it is (again) mitigated by a decrease in vertical diffusion. The net effect is a 0.31×10^{-6} mmol-N m^{-2} s^{-1} increase in NO_3^- uptake, with 57% of the deposited NO_3^- converted into extra production. The remainder mostly compensates for the reduction in upward vertical diffusion.

The balance between the terms of the budget is qualitatively different on the continental shelf of the MAB region (Table 1, Run 1). Vertical advection and vertical diffusion are about equally responsible for the NO_3^- inputs to the upper 15 m, while horizontal advection acts as a sink of smaller magnitude. The NO_3^- uptake term is the highest of the three regions (about twice that of the GS region) as expected from the higher nitrogen concentrations on the continental shelf (Section 5.3). Finally, the residual term is six times larger than in the other regions and again has no apparent seasonality (not shown).

Atmospheric deposition rates in the MAB are moderate (two thirds of the deposition in the GS region) but they have a significant effect on all budget terms (notably horizontal and vertical advection; Table 1). Changes in advective terms can be caused by changes in the 3-D currents, the NO_3^- concentrations, or both. In our case the currents are identical among the model runs and thus these changes indicate a modification (increase) in the mean NO_3^- fields (Section 5.3). This increase is apparent in the temporal derivative and indicates that the deposited nitrate is not immediately consumed in this region. Deposition causes a decrease in vertical diffusion (as in the GS and STG domain) that largely cancels the increase in advective inputs. The balance between advective and diffusive changes allows all of the deposited NO_3^- to be stored or used for extra production. This result contributes to the largest absolute gain in NO_3^- uptake of the three regions (Table 1). Overall, these NO_3^- budgets reveal important regional differences in the utilization of the deposited NO_3^-.

5.3 Impact of AND on surface nitrogen inventory

In this section we quantify the impact of atmospheric deposition on the nitrogen inventories of the upper 15 m, expanding on the regional differences discussed above and presenting the results in the form of time series to emphasize the strong seasonality. In the GS region, the NO_3^- concentrations of the control experiment exhibit a large seasonal cycle with highest values in winter (~ 3 mmol-N m^{-3}) and negligible concentrations dur-

ing the summer (Figure 5). Surface NH_4^+ concentrations have a similar seasonality, but with values of $\sim$ 0.2 mmol-N m^{-3} during the winter and $\sim$ 0.1 mmol-N m^{-3} during the summer. Semilabile DON generally increases during the period of biological production (March–May) and decreases afterward during its conversion to NH_4^+.

The effect of AND is relatively small in magnitude compared to the strong seasonal cycle of the biological fields in the GS region. For example, the relative increase in surface NO_3^- resulting from atmospheric deposition, computed as $(NO3_{\text{Run 2}} - NO3_{\text{Run 1}})/NO3_{\text{Run 1}}$, reveals that this deposited nitrogen has a negligible effect on the nitrogen inventory of the GS during the fall, winter and spring seasons (Figure 5). The nitrogen is sufficiently abundant during this period to overshadow the large deposition that characterizes the GS region (Figure 3).

The situation reverses in the GS region during the summer season when the stratification is maximum and the nitrogen inventory of the upper layers is at its minimum. Over the months of June–August in particular, the deposited nitrogen represents an increasingly large proportion of the nitrogen inventory (Figure 5). This pattern is most apparent for NO_3^- with peak increases of 80%. A large deposition event over the GS region can provide 1 mmol-N m^{-2} over a period of one day (Figure 6a). Once distributed over a depth of 15 m (comparable to the thickness of the uppermost model vertical level in deep water), this flux translates into a temporary increase in $NO_3^- + NH_4^+$ concentration of $1/15 \approx 0.07$ mmol-N m^{-3} (Figure 6b). This value is comparable with the 'nitrate patches' from rain events in the observational study of *Kodama et al.* [2011] (0.01–0.20 mmol-N m^{-3} at a depth of 4.5 m; See their Table 1). Such increases are short-lived in the GS region and concentrations typically fall back to pre-deposition levels after 1–2 days. The importance of the deposited N gradually decreases after August and becomes negligible in October when background concentrations rise again (Figure 5). The average increase in surface nitrogen concentrations during Jul.–Sep. (summer/late summer) is 14% for NO_3^-, 6.5% for NH_4^+, and 11% for DON (Table 2). These numbers are considerably lower when averaging over the entire year: 2%, 5% and 7.5%, respectively (Table 3).

The third experiment (Run 3) allows us to isolate the relative contributions of wet and dry atmospheric deposition. In all cases the wet deposition is responsible for the bulk of the nitrogen increases (Tables 2 and 3). In the GS region, wet deposition accounts for 66% of the changes in NO_3^- and 84% for NH_4^+. This proportion is consistent with the ratio of wet and dry deposition in this area (Figure 4).

The effect of AND in the STG region is qualitatively similar to the GS region. The deposited nitrogen becomes increasingly important from June to August before declining and becoming negligible by October (Figure 7). The increase in the summer inventory is 7% for NO_3^-, 2% for NH_4^+ and 10% for DON (Table 2). These values are lower than in the GS, as expected from the lower deposition rates of the STG (Figure 3).

This picture changes dramatically on the shelf of the MAB region (Figure 8). Nitrate concentrations remain $\geq$ 1 mmol-N m^{-3} during the summer period, which is comparable to the half-saturation coefficients for NO_3^- limitation (0.5 and 1 mmol-N m^{-3} for small/large phytoplankton, respectively; see Supporting Information). Ammonium concentrations are also relatively high throughout the year ($\sim$ 0.4 mmol-N m^{-3}) leading to an inhibition factor for NO_3^- uptake of $(1 + [NH4]/K_{NH4})^{-1} \sim 0.6$. These nitrate-replete conditions prevent the deposited nitrate from being immediately consumed and lead to surface concentrations that are constantly above those of the control simulation (+0.27 mmol-N m^{-3} on average in the MAB region; Table 3). This result is in stark contrast with the GS and STG regions where nitrogen is limiting and the deposited NO_3^- is often rapidly consumed.

The average increase in nitrogen concentrations in the MAB during summer (Jul.–Sep.) is 16% for NO_3^-, 15% for NH_4^+, and 6% for DON, which represents the largest in-

crease of the three regions (Table 2). These numbers remain significant when averaging over the entire year (8%, 7% and 4%, respectively; Table 3) and quantify the substantial effect of deposition on the mean nitrogen concentrations in the MAB.

5.4 Surface biological response to AND

In this section we examine the biological response in the upper 15 m of the three regions, again using time series to emphasize the important seasonality. Phytoplankton production and biomass in these regions typically exhibit a strong maximum in March–April corresponding to the spring bloom (Figures 5,7, and 8). Between one third and half of the primary production is from NO_3^- uptake while the remainder is from NH_4^+ (Tables 2 and 3).

In all three regions, AND generates the greatest biological response during the summer season (Figures 5,7 and 8), when the deposited nitrogen represents the largest fraction of the nitrogen inventory (cf. Section 5.3). The summer NO_3^- concentrations are sufficiently low in the GS and STG regions that the Michaelis-Menten functions can be linearized and the increase in NO_3^- uptake becomes roughly proportional to the deposited NO_3^- (Eq. 6). For example, in the GS region the 80% increase in NO_3^- concentration in August 2005 leads to an 80% increase in NO_3^- uptake (Figure 5). On average, the increase in NO_3^- uptake during the summer months is 19% for the GS and 9% for the STG (comparable to the increase in NO_3^- concentrations; cf. Section 5.3 and Table 2). The linearization is not valid in the MAB because of the more abundant nitrogen and the importance of NO_3^- uptake inhibition by NH_4^+. In this case, the relatively large summer increase in NO_3^- inventory (+16%) yields a comparatively modest increase in NO_3^- uptake (9%; Table 2, Figure 8).

Ammonium uptake is responsible for the bulk of the increase in total primary production (60–70% of the increase; see Tables 2 and 3). During the summer, the NH_4^+ uptake is increased by 17% in the GS region, 11% in the STG, and 9% in the MAB (Table 2). In the case of the GS and STG regions, the increase in NH_4^+ uptake is multiple times larger than the increase in NH_4^+ concentration (6.5% in GS and 2% in STG; cf. Section 5.3). Following Eq. 6, the increase in NH_4^+ uptake has to be driven by both increased NH_4^+ concentrations and increased phytoplankton abundance. For example, note the similarities between the green curves of chlorophyll and NH_4^+ uptake in Figures 5 and 7. Annually averaged values of NH_4^+ uptake show smaller increases (9%, 8% and 5% in the GS, STG, and MAB regions, respectively) as expected. Regarding chlorophyll concentrations in the upper 15 m, deposition causes a negligible increase from fall to spring but a substantial increase in July to September: 14% in the GS, 7% in the STG and 10% in the MAB (Table 2).

There is considerable spatial variability of primary production and chlorophyll as well as in the absolute and relative impact of atmospheric deposition on these quantities (Figures 9 and 10). The MAB region features the highest absolute increases in production resulting from AND (as expected from its high absolute increase in nitrogen concentrations). On the other hand, the high primary production and chlorophyll of the MAB implies relative increases that are comparatively small (Figures 9 and 10). The GS and STG regions exhibit the opposite pattern. These more oligotrophic regions are generally characterized by low productivity and chlorophyll concentrations, and thus although the absolute increases due to AND are low, the relative increases are high ($\geq$ 30%; Figures 9 and 10). Finally, some areas of the model domain show no increase at all, e.g., the Bay of Fundy or Georges Bank. We hypothesize that the year-round well-mixed conditions prevalent in these regions [*Garrett et al.*, 1978] limit surface accumulation of nitrogen and biomass.

5.5 Variations in the response of algal species

We now address differences in the biological response to AND between the two size classes of phytoplankton in the model (Figure 11). The smaller size class has lower nitrogen saturation coefficients and lower light requirements (Supporting Information). When combined with the large cross-shelf gradient in nitrogen concentrations (Supporting Information), the differences in the saturation coefficients generate a spatial segregation of the two size classes. The large phytoplankton are typically confined to the nitrogen-rich continental shelf and are generally present in only very low concentrations in the nitrogen-poor offshore regions (Figure 11b). The small phytoplankton are more ubiquitous with a weaker onshelf/offshelf gradient (Figure 11a).

This spatial segregation affects the response of the phytoplankton classes to atmospheric deposition since phytoplankton production is proportional to abundance (Eq. 4). For example, because the large phytoplankton are generally absent from the offshelf region, they show negligible increases from atmospheric deposition in this region (Figure 11d). The bulk of the increase in large phytoplankton occurs on the continental shelf where large phytoplankton biomass is greatest. In contrast, the small phytoplankton show a domain-wide increase in abundance in response to atmospheric deposition (Figure 11c).

Such variations in the response to deposition persist in regions where both size classes have comparable abundance. This is the case in the MAB region, where chlorophyll concentrations are on the order of 1 mg m^{-3} for both size classes during the summer (Figure 11a and b). Despite the similar abundances, the absolute increase in large phytoplankton is 2–3 times larger than for the small phytoplankton (Figure 11c and d). This difference results from the distinct saturation coefficients for the two size classes and the ambient nitrate/ammonium levels being close to these coefficients (Figure 8; Eq. 5). With its higher saturation coefficients, the large phytoplankton is more strongly bound by nitrogen availability and thus benefits more from atmospheric deposition. Moreover, the large phytoplankton is generally positioned higher in the water column (because of its higher light requirements) and again benefits more from the deposition at the surface.

5.6 Biological response below the surface

The effects of AND extend below the surface layer, particularly in July–September (summer/late summer) when the biological response to AND is strongest (cf. Section 5.4). The relative increases in NO_3^- and NH_4^+ caused by AND typically follow an exponential function with maximum change in the surface layer and negligible changes at 100 m depth (Figure 12a and b). The e-folding scale estimated from the profiles of relative change is $O(10\,\mathrm{m})$. The differences in nitrogen inventory change among the three regions (GS, STG, MAB) are the same as the differences in surface layer nitrogen change (cf. Section 5.3), with the largest change in the MAB and the smallest change in the STG (Figure 12a and b).

The profiles of primary production and chlorophyll also exhibit maximum changes in the surface layer and a gradual decrease with depth (Figure 12c and d). But in contrast with the nitrogen profiles, the change in production and chlorophyll eventually reaches negative values below a certain depth. In other words, AND would negatively impact the production and biomass below a certain depth. This behavior is absent from the STG regions, small in the GS region (−4%) and largest in the MAB region (up to −7%). The depth where the sign reverses is ∼ 15 m in the MAB and ∼ 50 m in the GS region.

Nitrogen concentrations generally show increases at all depths and thus cannot explain the decrease in deep primary production. The penetration of light, on the other hand, is negatively impacted by atmospheric deposition, which increases the chlorophyll and dissolved organic matter at the surface, leading to stronger light attenuation (k_d; see Supporting Information). The increase in k_d is largest in the MAB region (+4% in the upper

15 m on average during the summer) and smallest in the STG region (+0.3%). Note that the effect of a larger k_d is cumulative with depth: the amount of light available at 50 m is reduced by 14% in the MAB, 1.5% in the GS, and only 0.5% in the STG.

The decrease in deep production and deep chlorophyll has a minor impact on depth-integrated quantities since both fields are generally small below 60 m. During the summer, the depth-integrated primary productivity increases by 9% in the GS, 6% in the STG and 6% in the MAB. Similarly, the depth-integrated chlorophyll increases by 5% in the GS, 3% in the STG and 5% in the MAB during the summer. The relative increases in depth-integrated quantities are thus approximately half of their surface counterparts (Tables 2) and exhibit similar differences among the three regions (i.e. the largest relative increase is in the GS region). Annually averaged values are significantly lower than summer values: a 4%, 5% and 3% increase in primary productivity and a 3%, 4% and 2% increase in chlorophyll (in the GS, STG and MAB, respectively).

The relative increase in new depth-integrated production (Eq. 7) amounts to 22% in the GS, 14% in the STG, and 15% in the MAB during the summer. These values are larger than the relative increases in total production (cf. Section 5.4) because $PP^{\mathrm{NO3}}_{\mathrm{no\ deposition}}$ is only one third of the total production during the summer (Table 2). The annually averaged increase in new production is significantly lower (8% in the GS, 11% in the STG and 5% in the MAB) as expected.

6 Discussion and Summary

This study highlights the presence of a 'hot-spot' of AND over the Gulf Stream region (Figure 3a–c). The hot-spot can be partly explained by large anthropogenic sources of atmospheric nitrogen positioned directly upwind (west) of this area [e.g., *Paerl et al.*, 2002]. Another factor contributing to the localized maximum is the recurrent rainband over the Gulf Stream (*Hobbs* [1987] and Figure 3f). This interpretation is supported by the fact that dry deposition, which does not depend on precipitation, does not exhibit a strong maximum over the GS (Figures 3d and e).

The influence of the hot-spot on the local primary productivity is ultimately mitigated by physical and biogeochemical processes (Figure 13). Of these processes, the seasonal vertical stratification plays a key role by regulating the vertical nitrogen supply and the background surface nitrogen inventory. AND is only found to be significant during the summer period when the stratification is maximal and prohibits vertical diffusion of high-nitrogen waters to the surface, thus resulting in relatively low background nitrogen levels [*Myriokefalitakis et al.*, 2016]. Another physical mechanism that limits the biological impact of AND is the reduction in upward nitrogen diffusion. As AND increases surface nitrogen concentrations, the gradient in the upper 20 m is reduced, which ultimately results in a decreased rate of vertical nitrogen diffusion. This negative feedback is observed in the three regions of our model domain and partly cancels the nitrogen enrichment of AND. Finally, this study highlights how increased surface chlorophyll resulting from the nitrogen enrichment of AND leads to a reduction in light availability at depth in the MAB. This biogeochemical feedback again partially mitigates the impact of AND by decreasing the net impact on depth-integrated primary production.

Despite these negative feedbacks, the gains in primary production remain significant. The annually averaged increases in new depth-integrated production generated by our modeling system (Section 5.6) are in broad agreement with the estimates of *Kim et al.* [2014b] (7–15% for the offshelf region and 1–2% on the coastal shelf). Although these changes may be difficult to distinguish from natural variability in observations, they suggest that AND is increasing the carbon export in coastal regions impacted by human activities. However, our model study suggests interesting differences in the way AND affects small and large phytoplankton. Phytoplankton that are positioned in the upper part of the

water column and have higher nitrogen requirements appear to benefit more from AND. The contrasted response between the two size classes highlights the importance of multiple plankton classes in biogeochemical and food web models [*Ford et al.*, 2016; *Xiao and Friedrichs*, 2014a]. On the other hand, the model underestimation of chlorophyll concentrations along the coasts (Supporting Information) suggests that primary production in the nearshore region may not be well represented by the current model. The bias could be a reflection of the coarse horizontal resolution (9 km) or a suboptimal choice of the biogeochemical parameters affecting primary production.

Anthropogenic nitrogen emissions have varied substantially over past decades, with a decline in oxidized nitrogen and an increase in reduced nitrogen in the eastern US [*Paerl et al.*, 2002; *Li et al.*, 2016; *Linker et al.*, 2013; *Dennis*, 2012]. These trends are generally attributed to a reduction in the emissions from power plants and mobile sources (following the Clean Air Act) and to increased inputs from agricultural activities (respectively). Extrapolating the trend in the CMAQ data (~ -0.2 mmol-N m^{-2} month^{-1} per year, from 2002 to 2010) back to 1990 would roughly increase the AND over the Gulf Stream region by 40%. It remains unclear whether such large fluxes could increase the new production by $1.4 \times 22\% \approx 30\%$ in the GS region during the summer (relative to a control simulation devoid of AND; cf. Section 5.6) or if the aforementioned feedback processes [and limitation by other nutrients; e.g., *Kim et al.*, 2014a] would limit the changes to the biological pump. For example, incubation experiments recently conducted off the continental shelf of the Mid-Atlantic Bight show that nitrogen is the proximate limiting nutrient for phytoplankton growth with a secondary limitation by phosphorus availability (P. N. Sedwick, personal communication, 2017). Limitation by phosphorus may thus play a role in mitigating the effect of AND. The temporal coverage of the present study (2004–2008) would need to be expanded to capture the ecological significance of such long-term changes.

Recent studies have highlighted the importance of certain biogeochemical processes that are not explicitly represented in the present model. *Somes et al.* [2016] show that AND is accompanied by a reduction in nitrogen fixation by diazotrophs and an increase in water-column denitrification. These two negative feedbacks effectively buffer the increase in global marine productivity. However, these feedbacks appear to be concentrated in the tropical portion of the North Atlantic and in oxygen-poor aphotic zones (respectively). Their impact on the near-surface productivity of the US east coast is thus expected to be minor. Another open question concerns the role of organic nitrogen in AND. Wet organic nitrogen deposition is only parameterized in the present study while dry organic nitrogen deposition is neglected altogether (because of insufficient data). Moreover, recent evidence from Bermuda suggests that ammonium in rainwater and organic N in rainwater and aerosols primarily have a marine source [*Altieri et al.*, 2014, 2016]. Unfortunately this two-way exchange of nitrogen between the atmosphere and ocean (e.g., via NH_3 gas exchange) cannot be easily incorporated into our modeling framework for two reasons. First, CMAQ does not currently include nitrogen emissions from the ocean. Second, in order to properly include the two-way exchange of nitrogen between the atmosphere and ocean, we would have to couple the atmosphere and ocean models and run them simultaneously. Such a coupling should be considered in future modeling studies.

Acknowledgments

This research was supported by the National Science Foundation (collaborative grants OCE-1259187 and OCE-1260574). This work was performed using High Performance Computing facilities at the College of William & Mary, which were provided by contributions from the National Science Foundation, the Commonwealth of Virginia Equipment Trust Fund and the Office of Naval Research. We thank the reviewers for their helpful comments. We also thank Donna B. Schwede from the Environmental Protection Agency's Office of Research and Development for contributing the CMAQ data. The data from this study will be permanently archived and publicly available on W&M Publish (`http://publish.wm.edu/`)

after the manuscript is accepted. This paper is Contribution No. xxxx of the Virginia Institute of Marine Science, College of William & Mary.

References

Altieri, K. E., M. G. Hastings, A. J. Peters, S. Oleynik, and D. M. Sigman (2014), Isotopic evidence for a marine ammonium source in rainwater at Bermuda, *Global Biogeochemical Cycles*, *28*, 1066–1080, doi:10.1002/2014GB004809.

Altieri, K. E., S. E. Fawcett, A. J. Peters, D. M. Sigman, and M. G. Hastings (2016), Marine biogenic source of atmospheric organic nitrogen in the subtropical North Atlantic, *Proceedings of the national academy of sciences*, p. 6, doi:10.1073/pnas.1516847113.

Appel, K. W., K. M. Foley, J. O. Bash, R. W. Pinder, R. L. Dennis, D. J. Allen, and K. Pickering (2011), A multi-resolution assessment of the Community Multiscale Air Quality (CMAQ) model v4.7 wet deposition estimates for 2002-2006, *Geoscientific Model Development*, *4*, 357–371, doi:10.5194/gmd-4-357-2011.

Appel, K. W., G. A. Pouliot, H. Simon, G. Sarwar, H. Pye, S. L. Napelenok, F. Akhtar, and S. J. Roselle (2013), Evaluation of dust and trace metal estimates from the Community Multiscale Air Quality (CMAQ) model version 5.0, *Geosci. Model Dev.*, *6*, 883–899, doi:10.5194/gmd-6-883-2013.

Bash, J. O., E. J. Cooter, R. L. Dennis, J. Walker, and J. E. Pleim (2013), Evaluation of a regional air-quality model with bi-directional NH_3 exchange coupled to an agroecosystem model, *Biogeosciences*, *10*, 1635–1645, doi:10.5194/bg-10-1635-2013.

Behrenfeld, M. J., R. T. O'Malley, D. A. Siegel, C. R. McClain, J. L. Sarmiento, G. C. Feldman, A. J. Milligan, P. G. Falkowski, R. M. Letelier, and E. S. Boss (2006), Climate-driven trends in contemporary ocean productivity, *Nature*, *444*, 752–755, doi:10.1038/nature05317.

Boyer, T., J. I. Antonov, O. K. Baranova, C. Coleman, H. E. Garcia, A. Grodsky, D. R. Johnson, R. A. Locarnini, A. V. Mishonov, T. D. O'Brien, C. Paver, J. Reagan, D. Seidov, I. V. Smolyar, and M. M. Zweng (2013), World ocean database 2013, NOAA Atlas NESDIS 72, doi:10.7289/V5NZ85MT.

Cahill, B., J. Wilkin, K. Fennel, D. Vandemark, and M. A. M. Friedrichs (2016), Interannual and seasonal variability in air-sea CO_2 fluxes along the U.S. Eastern Continental Shelf and their sensitivity to increasing air temperatures and variable winds, *J. Geophys. Res. Biogeosciences*, *121*, doi:10.1002/2015JG002939.

Canty, T. P., L. Hembeck, T. P. Vinciguerra, D. C. Anderson, D. L. Goldberg, S. F. Carpenter, D. J. Allen, C. P. Loughner, R. J. Salawitch, and R. R. Dickerson (2015), Ozone and NOx chemistry in the eastern US: Evaluation of CMAQ/CB05 with satellite (OMI) data, *Atmos. Chem. Phys.*, *15*, 10,965–10,982, doi:10.5194/acp-15-10965-2015.

Cornell, S. E., T. D. Jickells, J. Cape, A. P. Rowland, and R. A. Duce (2003), Organic nitrogen deposition on land and coastal environments: A review of methods and data, *Atmospheric Environment*, *37*(16), 2173–2191, doi:10.1016/S1352-2310(03)00133-X.

Cummings, J. A. (2005), Operational multivariate ocean data assimilation, *J. R. Meteorol. Soc.*, *131*, 3583–3604.

Dee, D. P., S. M. Uppala, A. J. Simmons, P. Berrisford, P. Poli, S. Kobayashi, U. Andrae, M. A. Balmaseda, G. Balsamo, P. Bauer, P. Bechtold, A. C. M. Beljaars, L. van de Berg, J. Bidlot, N. Bormann, C. Delsol, R. Dragani, M. Fuentes, A. J. Geer, L. Haimberger, S. B. Healy, H. Hersbach, E. V. Holm, L. Isaksen, P. Kallberg, M. Kohler, M. Matricardi, A. P. McNally, B. M. Monge-Sanz, J.-J. Morcrette, B.-K. Park, C. Peubey, P. de Rosnay, C. Tavolato, J.-N. Thepaut, and F. Vitart (2011), The ERA-Interim reanalysis: Configuration and performance of the data assimilation system, *Quarterly Journal of the Royal Meteorological Society*, *137*, 553–597, doi:10.1002/qj.828.

Dennis, R. (2012), Total inorganic nitrogen deposition, in *Albemarle-Pamlico Ecosystem Assessment*, edited by D. E. Carpenter and L. Dubbs, pp. 67–72, Albemarle-Pamlico

National Estuary Partnership, Raleigh, NC.

Doney, S. C., N. Mahowald, I. Lima, R. A. Feely, F. T. Mackenzie, J. Lamarque, and P. J. Rasch (2007), Impact of anthropogenic atmospheric nitrogen and sulfur deposition on ocean acidification and the inorganic carbon system, *Proceedings of the national academy of sciences*, *104*(37), 14,580–14,585, doi:10.1073/pnas.0702218104.

Druon, J., A. Mannino, S. Signorini, C. McClain, M. A. M. Friedrichs, J. Wilkin, and K. Fennel (2010), Modeling the dynamics and export of dissolved organic matter in the Northeastern US continental shelf, *Estuarine Coastal and Shelf Science*, *88*(4), 488–507, doi:10.1016/j.ecss.2010.05.010.

Duce, R. A., J. LaRoche, K. Altieri, K. R. Arrigo, A. R. Baker, D. G. Capone, S. Cornell, F. Dentener, J. Galloway, R. S. Ganeshram, R. J. Geider, T. Jickells, M. M. Kuypers, R. Langlois, P. S. Liss, S. M. Liu, J. J. Middelburg, C. M. Moore, S. Nickovic, A. Oschlies, T. Pedersen, J. Prospero, R. Schlitzer, S. Seitzinger, L. L. Sorensen, M. Uematsu, O. Ulloa, M. Voss, B. Ward, and L. Zamora (2008), Impacts of atmospheric anthropogenic nitrogen on the open ocean, *Science*, *320*(5878), 893–897, doi:10.1126/science.1150369.

Eder, B., J. Bash, K. Foley, and J. Pleim (2014), Incorporating principal component analysis into air quality model evaluation, *Atmospheric Environment*, *82*, 307–315, doi:10.1016/j.atmosenv.2013.10.015.

Egbert, G. D., and S. Y. Erofeeva (2002), Efficient inverse modeling of barotropic ocean tides, *J. Atmos. Oceanic Technol.*, *19*, 183–204, doi:10.1175/1520-0426(2002)019<0183:EIMOBO>2.0.CO;2.

Fairall, C. W., E. F. Bradley, J. E. Hare, A. A. Grachev, and J. B. Edson (2003), Bulk parameterization of air-sea fluxes: Updates and verification for the COARE algorithm, *J. Clim.*, *16*, 571–591.

Fennel, K., J. Wilkin, J. Levin, J. Moisan, J. O'Reilly, and D. Haidvogel (2006), Nitrogen cycling in the Middle Atlantic Bight: Results from a three-dimensional model and implications for the North Atlantic nitrogen budget, *Global Biogeochemical Cycles*, *20*(GB3007), doi:10.1029/2005GB002456.

Fennel, K., J. Wilkin, M. Previdi, and R. Najjar (2008), Denitrification effects on air-sea CO2 flux in the coastal ocean: Simulations for the northwest North Atlantic, *Geophys. Res. Lett.*, *35*(24), doi:10.1029/2008gl036147.

Ford, D. A., J. van der Molen, K. Hyder, J. Bacon, R. Barciela, V. Creach, R. McEwan, P. Ruardij, , and R. Forster (2016), Observing and modelling phytoplankton community structure in the North Sea: can ERSEM-type models simulate biodiversity?, *Biogeosciences Discussion*, doi:10.5194/bg-2016-304.

Gantt, B., J. T. Kelly, and J. Bash (2015), Updating sea spray aerosol emissions in the Community Multiscale Air Quality (CMAQ) model version 5.0.2, *Geosci. Model Dev.*, *8*, 3733–3746, doi:10.5194/gmd-8-3733-2015.

Garcia, H. E., and L. I. Gordon (1992), Oxygen solubility in seawater: Better fitting equations, *Limnology and oceanography*, *37*(6), 1307–1312.

Garrett, C. J., J. R. Keeley, and D. A. Greenberg (1978), Tidal mixing versus thermal stratification in the Bay of Fundy and Gulf of Maine, *Atmosphere-Ocean*, *16*(4), 403–423, doi:10.1080/07055900.1978.9649046.

Henrichs, S. M., and W. S. Reeburgh (1987), Anaerobic mineralization of marine sediment organic matter: Rates and the role of anaerobic processes in the oceanic carbon economy, *Geomicrobiology Journal*, *5*(3-4), 191–237, doi:10.1080/01490458709385971.

Hobbs, P. V. (1987), The Gulf Stream rainband, *Geophys. Res. Lett.*, *14*(11), 1142–1145.

Hofmann, E. E., J. Druon, K. Fennel, M. A. M. Friedrichs, D. Haidvogel, C. Lee, A. Mannino, C. McClain, R. Najjar, J. O'Reilly, D. Pollard, M. Previdi, S. Seitzinger, J. Siewert, S. Signorini, and J. Wilkin (2008), Eastern US continental shelf carbon budget: Integrating models, data assimilation and analysis, *Oceanography*, *21*, 32–40.

Hofmann, E. E., B. Cahill, K. Fennel, M. A. M. Friedrichs, K. Hyde, C. Lee, A. Mannino, R. G. Najjar, J. E. O'Reilly, J. Wilkin, and J. Xue (2011), Modeling the dynamics

of continental shelf carbon, *Annu. Rev. Marine Sci.*, *3*, 93–122, doi:10.1146/annurev-marine-120709-142740.

Huffman, G. J., R. F. Adler, D. T. Bolvin, G. Gu, E. J. Nelkin, K. P. Bowman, Y. Hong, E. F. Stocker, and D. B. Wolff (2007), Multi-satellite precipitation analysis: Quasi-global, multi-year, combined-sensor precipitation estimates at fine scale, *J. Hydrometeor.*, *8*, 38–55.

Jickells, T., A. R. Baker, J. N. Cape, S. E. Cornell, and E. Nemitz (2013), The cycling of organic nitrogen through the atmosphere, *Phil. Trans. R. Soc. B: Biological Sciences*, *368*(20130115), doi:10.1098/rstb.2013.0115.

Kim, I., K. Lee, N. Gruber, D. M. Karl, J. L. Bullister, S. Yang, and T. Kim (2014a), Increasing anthropogenic nitrogen in the North Pacific Ocean, *Science*, *346*(6213), 1102–1106, doi:10.1126/science.1258396.

Kim, T., K. Lee, R. G. Najjar, H. Jeong, and H. J. Jeong (2011), Increasing N abundance in the Northwestern Pacific Ocean due to atmospheric nitrogen deposition, *Science*, *334*, 505–509, doi:10.1126/science.1206583.

Kim, T., R. G. Najjar, and K. Lee (2014b), Influence of precipitation events on phytoplankton biomass in coastal waters of the eastern United States, *Global Biogeochemical Cycles*, *28*, 1–13, doi:10.1002/2013GB004712.

Kodama, T., K. Furuya, F. Hashihama, S. Takeda, and J. Kanda (2011), Occurrence of rain-origin nitrate patches at the nutrient-depleted surface in the East China Sea and the Philippine Sea during summer, *J. Geophys. Res. Oceans*, *116*(C08003), doi:10.1029/2010JC006814.

Krishnamurthy, A., J. K. Moore, C. S. Zender, and C. Luo (2007), Effects of atmospheric inorganic nitrogen deposition on ocean biogeochemistry, *J. Geophys. Res. Biogeosciences*, *112*(G02019), 10, doi:10.1029/2006JG000334.

Li, Y., B. A. Schichtel, J. T. Walker, D. B. Schwede, X. Chen, C. M. Lehmann, M. A. Puchalski, D. A. Gaye, and J. L. Collett (2016), Increasing importance of deposition of reduced nitrogen in the United States, *Proceedings of the National Academy of Sciences of the United States of America*, *113*(21), 5874–5879, doi:10.1073/pnas.1525736113.

Linker, L. C., R. Dennis, G. W. Shenk, R. A. Batiuk, J. Grimm, and P. Wang (2013), Computing atmospheric nutrient loads to the Chesapeake Bay watershed and tidal waters, *J. American Water Resources Assoc.*, *49*(5), doi:10.1111/jawr.12112.

Martins, D. K., R. G. Najjar, M. Tzortziou, N. Abuhassan, A. M. Thompson, and D. E. Kollonige (2016), Spatial and temporal variability of ground and satellite column measurements of NO_2 and O_3 over the Atlantic Ocean during the Deposition of Atmospheric Nitrogen to Coastal Ecosystems experiment, *J. Geophys. Res. Atmos.*, *121*(14), 14,175–14,187, doi:10.1002/2016JD024998.

Mellor, G. L., and T. Yamada (1982), Development of a turbulence closure model for geophysical fluid problems, *Reviews of geophysics and space physics*, *20*(4), 851–875.

Mesinger, F., G. DiMego, E. Kalnay, K. Mitchell, P. C. Shafran, W. Ebisuzaki, D. Jovic, J. Woollen, E. Rogers, E. H. Berbery, M. B. Ek, Y. Fan, R. Grumbine, W. Higgins, H. Li, Y. Lin, G. Manikin, D. Parrish, and W. Shi (2006), North American Regional Reanalysis: A long-term, consistent, high-resolution climate dataset for the North American domain, as a major improvement upon the earlier global reanalysis datasets in both resolution and accuracy, *Bull. Amer. Meteor. Soc.*, *87*, 343–360.

Meyers, T. P., P. Finkelstein, J. Clarke, T. G. Ellestad, and P. F. Sims (1998), A multilayer model for inferring dry deposition using standard meteorological measurements, *J. Geophys. Res. Atmos.*, *103*, 22,645–22,661.

Myriokefalitakis, S., A. Nenes, A. R. Baker, N. Mihalopoulos, and M. Kanakidou (2016), Bioavailable atmospheric phosphorous supply to the global ocean: A 3-D global modeling study, *Biogeosciences*, *13*, 6519–6543, doi:10.5194/bg-13-6519-2016.

NASA (2014), SeaWiFS level-3 standard mapped image at 9 km resolution (OC4 algorithm), NASA Goddard Space Flight Center, Ocean Ecology Laboratory, Ocean Biology Processing Group.

Paerl, H. W. (1995), Coastal eutrophication in relation to atmospheric nitrogen deposition: Current perspectives, *Ophelia*, *41*, 237–259.

Paerl, H. W., J. D. Willey, M. Go, B. L. Peierls, J. L. Pinckney, and M. L. Fogel (1999), Rainfall stimulation of primary production in western Atlantic Ocean waters: Roles of different nitrogen sources and co-limiting nutrients, *Marine Ecology Progress Series*, *76*, 205–214.

Paerl, H. W., R. L. Dennis, and D. R. Whitall (2002), Atmospheric deposition of nitrogen: Implications for nutrient over-enrichment of coastal waters, *Estuaries*, *25*(4b), 677–693.

Peierls, B. J., and H. W. Paerl (1997), Bioavailability of atmospheric organic nitrogen deposition to coastal phytoplankton, *Limnol. Oceanogr.*, *42*(8), 1819–1823.

Peterson, E. L. (1999), Benthic shear stress and sediment condition, *Aquacultural Engineering*, *21*(2), 85–111, doi:10.1016/S0144-8609(99)00025-4.

Rhein, M., S. R. Rintoul, S. Aoki, E. Campos, D. Chambers, R. A. Feely, S. Gulev, G. C. Johnson, S. A. Josey, A. Kostianoy, C. Mauritzen, D. Roemmich, L. D. Talley, and F. Wang (2013), Observations: Ocean, in *Climate Change 2013: The Physical Science Basis. Contribution of Working Group I to the Fifth Assessment Report of the Intergovernmental Panel on Climate Change*, chap. Stocker, T.F., D. Qin, G.-K. Plattner, M. Tignor, S.K. Allen, J. Boschung, A. Nauels, Y. Xia, V. Bex and P.M. Midgley (eds.), Cambridge University Press, Cambridge, United Kingdom and New York, NY, USA.

Sarwar, G., K. W. Appel, A. G. Carlton, R. Mathur, K. Schere, R. Zhang, and M. A. Majeed (2011), Impact of a new condensed toluene mechanism on air quality model predictions in the US, *Geosci. Model Dev.*, *4*, 183–193, doi: 10.5194/gmd-4-183-2011.

Schwede, D. B., and G. Lear (2014), A novel hybrid approach for estimating total deposition in the United States, *Atmospheric Environment*, *92*, 207–220, doi:10.1016/j.atmosenv.2014.04.008.

Shchepetkin, A. F., and J. C. McWilliams (2005), The Regional Oceanic Modeling System (ROMS): A split-explicit, free-surface, topography-following-coordinate oceanic model, *Ocean Model.*, *9*, 347–404, doi:10.1016/j.ocemod.2004.08.002.

Skamarock, W. C., J. B. Klemp, J. Dudhia, D. O. Gill, D. M. Barker, M. G. Dudha, X. Huang, W. Wang, and Y. Powers (2008), A description of the advanced research WRF Version 30, NCAR technical note, *Tech. rep.*, NCAR/TN-475.

Smolarkiewicz, P. K., and L. G. Margolin (1998), MPDATA: A finite difference solver for geophysical flows, *J. Comput. Phys.*, *140*, 459–480.

Somes, C. J., A. Landolfi, W. Koeve, and A. Oschlies (2016), Limited impact of atmospheric nitrogen deposition on marine productivity due to biogeochemical feedbacks in a global ocean model, *Geophys. Res. Lett.*, *43*, 4500–4509, doi:10.1002/2016GL068335.

Wang, R., Y. Balkanski, L. Bopp, O. Aumont, O. Boucher, P. Ciais, M. Gehlen, J. Penuelas, C. Ethe, D. Hauglustaine, B. Li, J. Liu, F. Zhou, and S. Tao (2015), Influence of anthropogenic aerosol deposition on the relationship between oceanic productivity and warming, *Geophys. Res. Lett.*, *42*, 10,745–10,754, doi:10.1002/2015GL066753.

Wanninkhof, R. (1992), Relationship between wind speed and gas exchange over the ocean, *J. Geophys. Res.*, *97*(C5), 7373–7382, doi:10.1029/92JC00188.

Weiss, R. F. (1974), Carbon dioxide in water and seawater: The solubility of a non-ideal gas, *Marine Chemistry*, *2*(3), 203–215, doi:10.1016/0304-4203(74)90015-2.

Xiao, Y., and M. A. M. Friedrichs (2014a), Using biogeochemical data assimilation to assess the relative skill of multiple ecosystem models in the Mid-Atlantic Bight: effects of increasing the complexity of the planktonic food web, *Biogeosciences*, *11*, 3015–3030, doi:10.5194/bg-11-3015-2014.

Xiao, Y., and M. A. M. Friedrichs (2014b), The assimilation of satellite-derived data into a one-dimensional lower trophic level marine ecosystem model, *J. Geophys. Res. Oceans*, *119*, 2691–2712, doi:10.1002/2013JC009433.

Zeebe, R. E., and D. Wolf-Gladrow (2001), *CO_2 in seawater: Equilibrium, kinetics, isotopes*, vol. 65, 346 pp., Elsevier Ocenographic Series.

Zhang, Y., L. Song, X. J. Liu, W. Q. Li, S. H. Lu, L. X. Zheng, Z. C. Bai, G. Y. Cai, and F. S. Zhang (2012), Atmospheric organic nitrogen deposition in China, *Atmospheric Environment*, *46*, 195–204, doi:10.1016/j.atmosenv.2011.09.080.

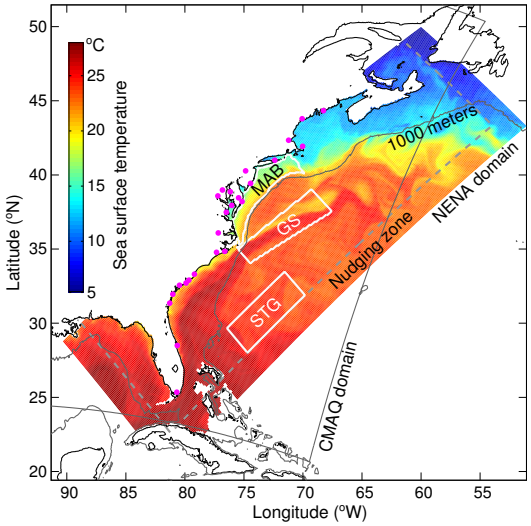

Figure 1. Extent of the oceanic (NENA) and atmospheric (CMAQ) model domains. GS: Gulf Stream, STG: Sub-Tropical Gyre, MAB: Mid-Atlantic Bight. The three boxes represent the regions used in the analyses. Note that the MAB region does not include the Chesapeake/Delaware bays nor Long Island Sound. Sea surface temperature represents a snapshot from the model on Nov. 5, 2003. The model nudging zones are indicated by the dashed line. The magenta dots represent the 25 stations used in the evaluation of CMAQ (see Figure 2).

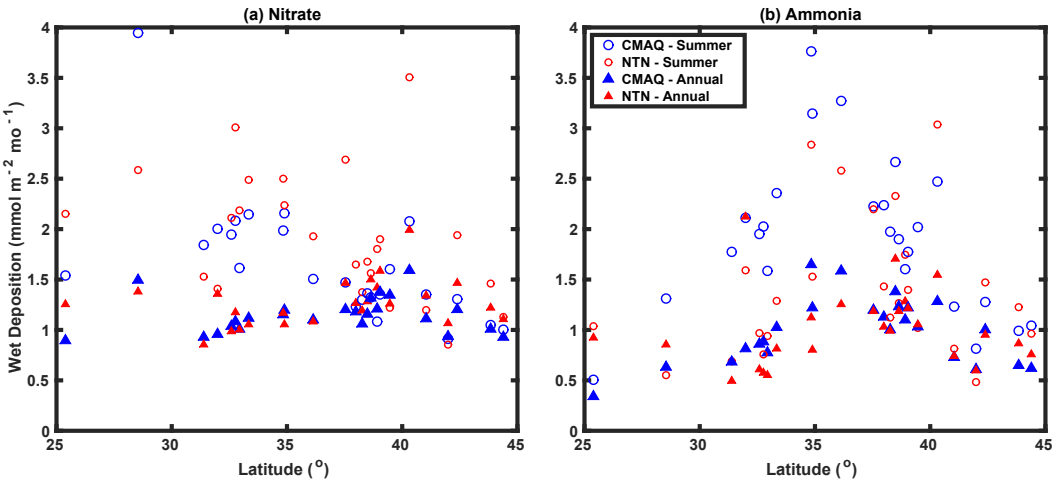

Figure 2. Observed and CMAQ-simulated wet deposition as a function of latitude at NTN sites within 50 km of the US east coast (25 sites total; see Figure 1). (a) Comparison between wet deposition of NO_3^- and HNO_3 (CMAQ) versus NO_3^- (NTN). (b) Comparison between wet deposition of NH_4^+ and NH_3 (CMAQ) versus NH_4^+ (NTN). Averages were made for 2004 to 2008 for the annual and summer (June–August) time periods.

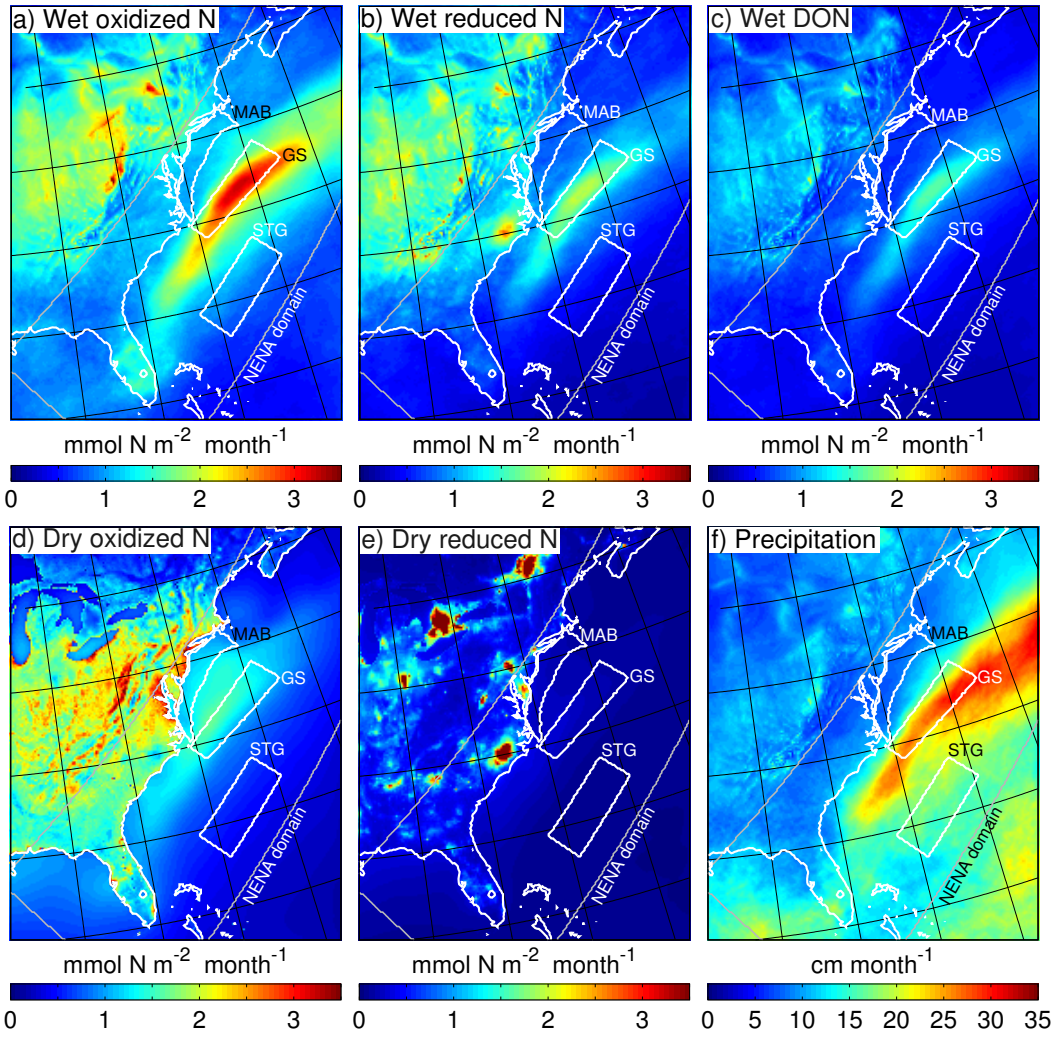

Figure 3. Spatial variability of atmospheric nitrogen deposition from the atmospheric chemistry model (average 2004–2008). (a,b,c) Wet deposition and (d,e) dry deposition. (f) Mean precipitation from CMAQ (average 2004–2008). See section 2.1 for the list of nitrogen species included in oxidized/reduced categories. The black lines indicate longitude and latitude every 5°. The gray rectangle is the oceanic model domain (NENA). The three white boxes represent the three regions analyzed (GS, STG, MAB).

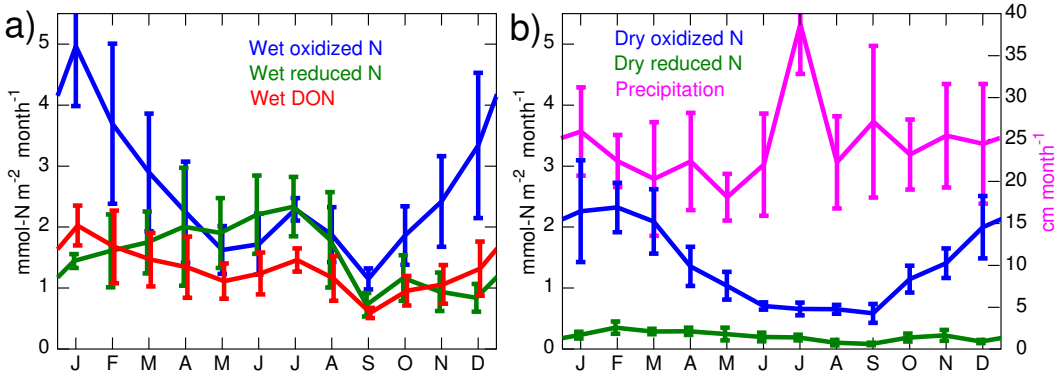

Figure 4. Seasonal variability of atmospheric nitrogen deposition over the Gulf Stream region (GS, Figure 1, years 2004 to 2008). See section 2.1 for the list of nitrogen species included in oxidized/reduced categories. The bars are standard deviations calculated from monthly values for 2004–2008.

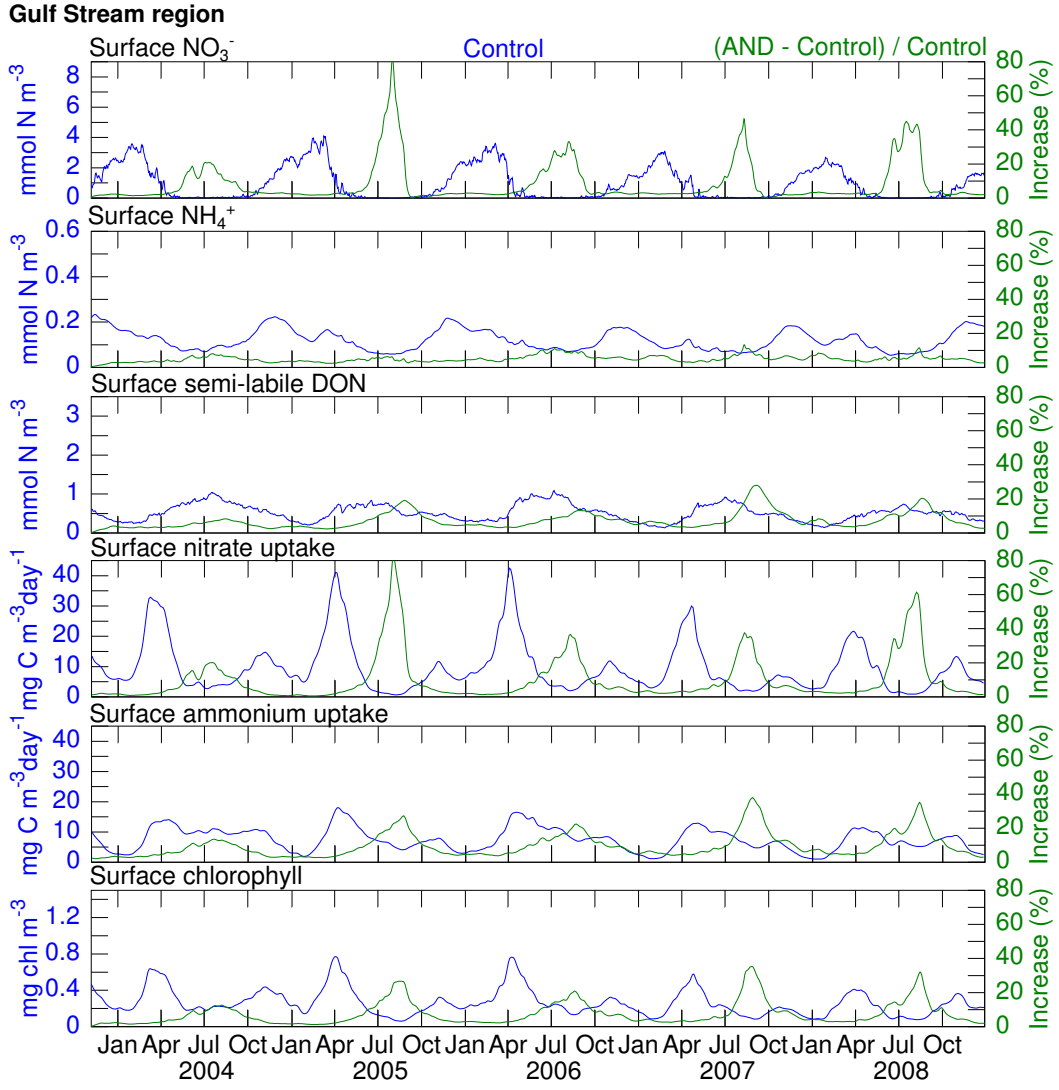

Figure 5. Time-variability of the response to atmospheric nitrogen deposition in the upper 15 m of the Gulf Stream region (GS, Figure 1). Blue curves represent the control (Run 1) while green curves represent the relative increase due to wet+dry deposition; (Run 2 − Run 1)/Run 1. The time-series are low-pass filtered for clarity.

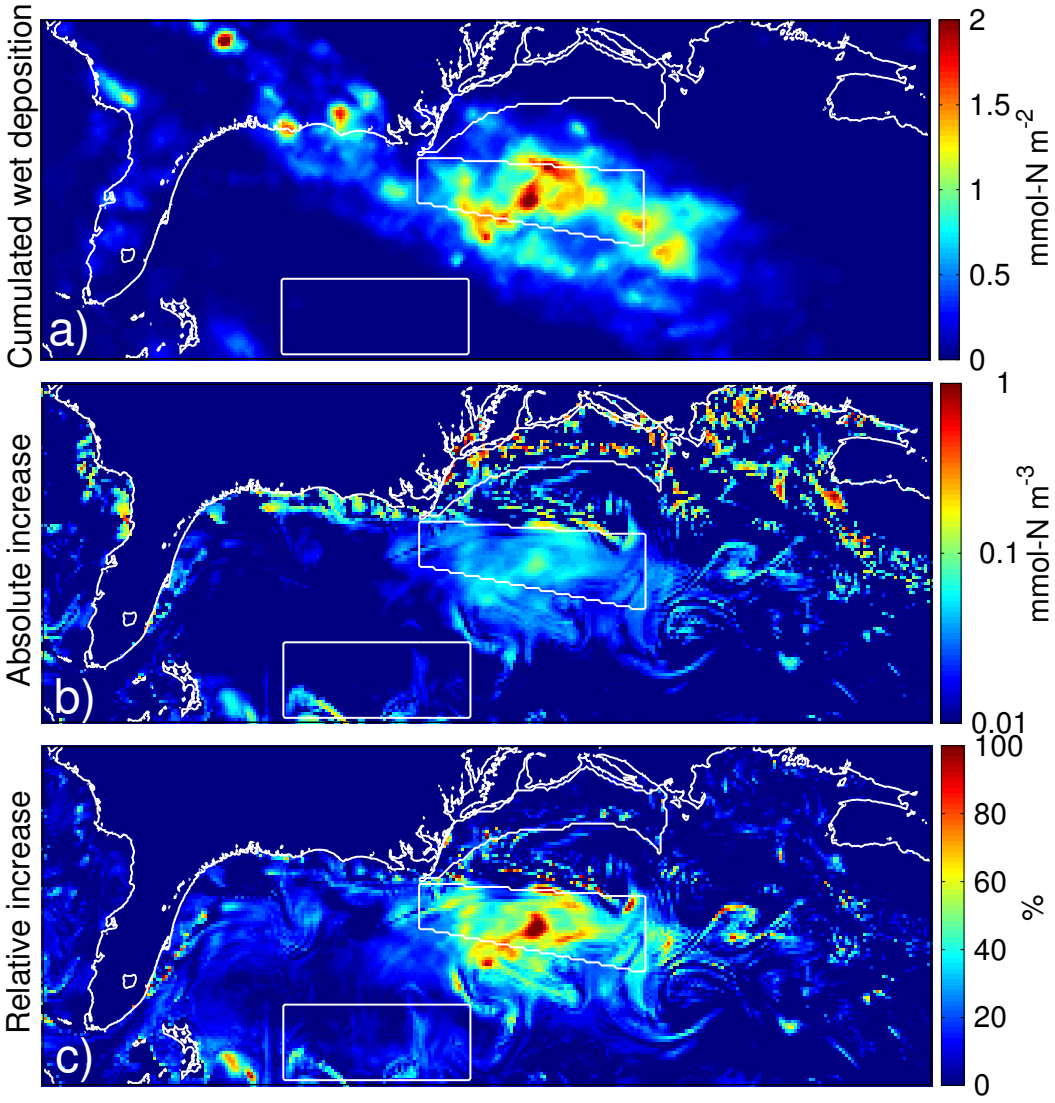

Figure 6. Example of a large wet deposition event simulated by the model. (a) Wet deposition of oxidized and reduced nitrogen cumulated between Aug. 23 19:30 and Aug. 24 19:30 (year 2005). (b) Absolute increase in $NO_3^- + NH_4^+$ between Aug. 24 7:30 and Aug. 25 7:30 (year 2005). The concentrations are averaged over the upper 15 m. (c) Same as (b) but showing the relative increase. The control simulation does not exhibit such an increase during this period (not shown) confirming that deposition is the cause of the increased concentrations.

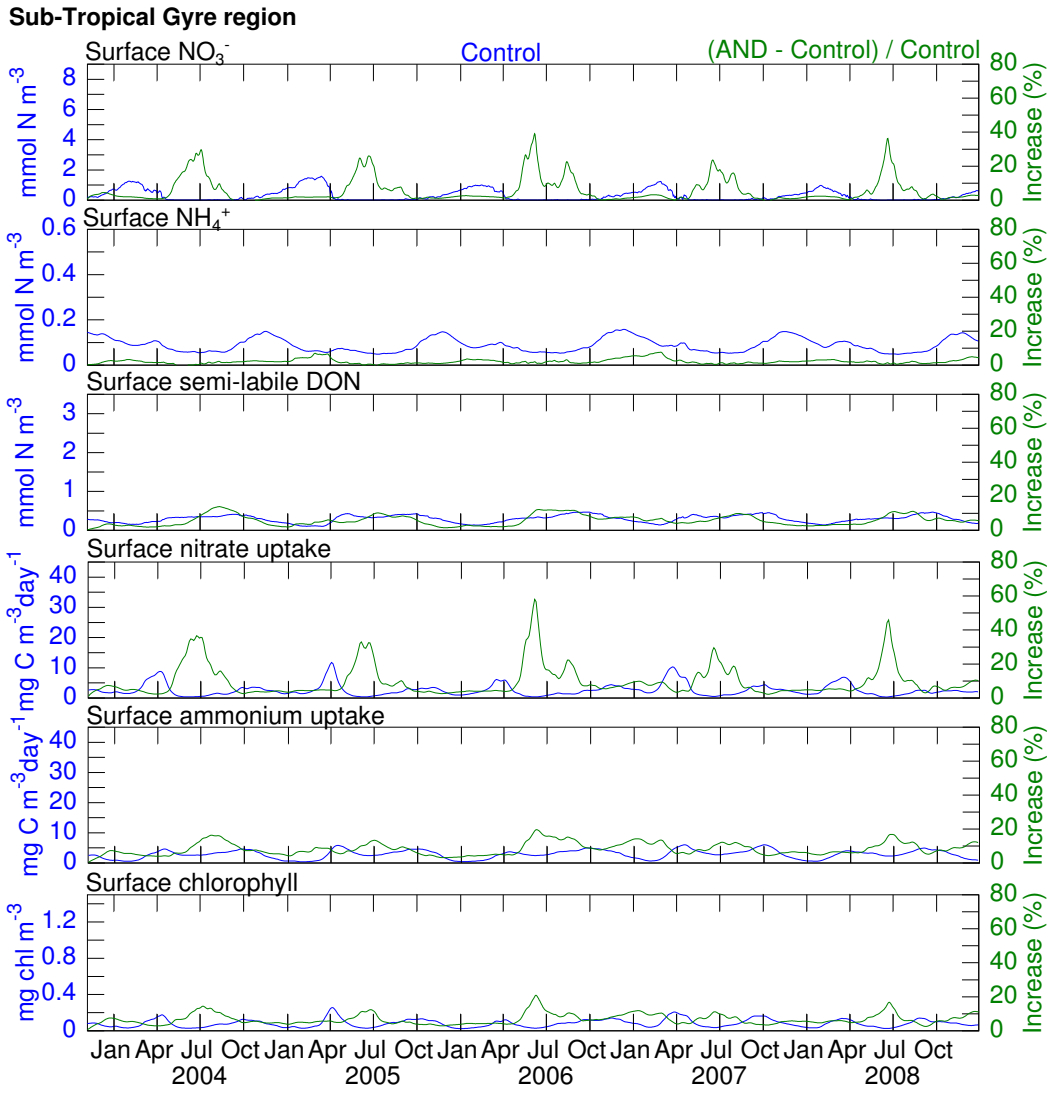

Figure 7. Same as Figure 5 but for the Sub-Tropical Gyre (STG).

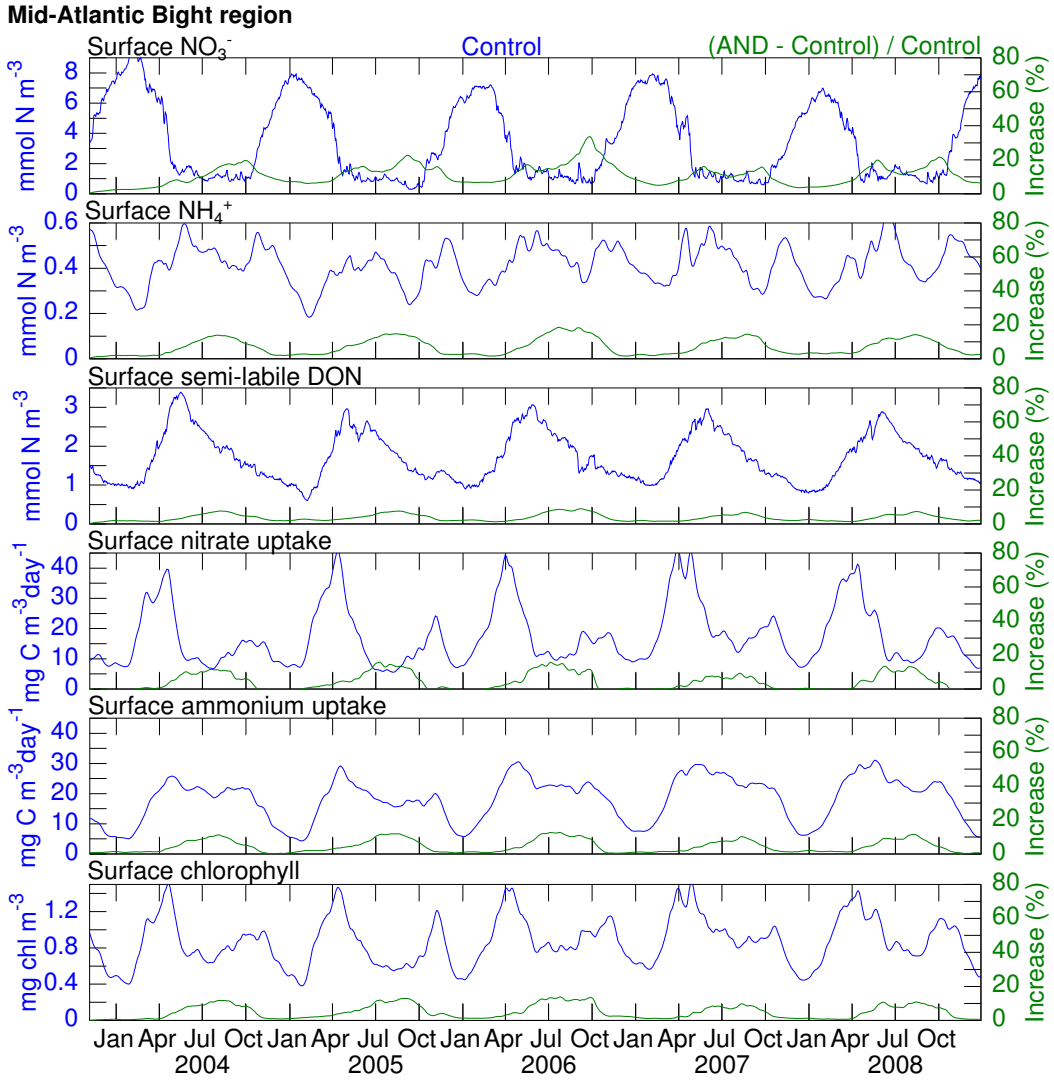

Figure 8. Same as Figure 5 but for the Mid-Atlantic Bight (MAB).

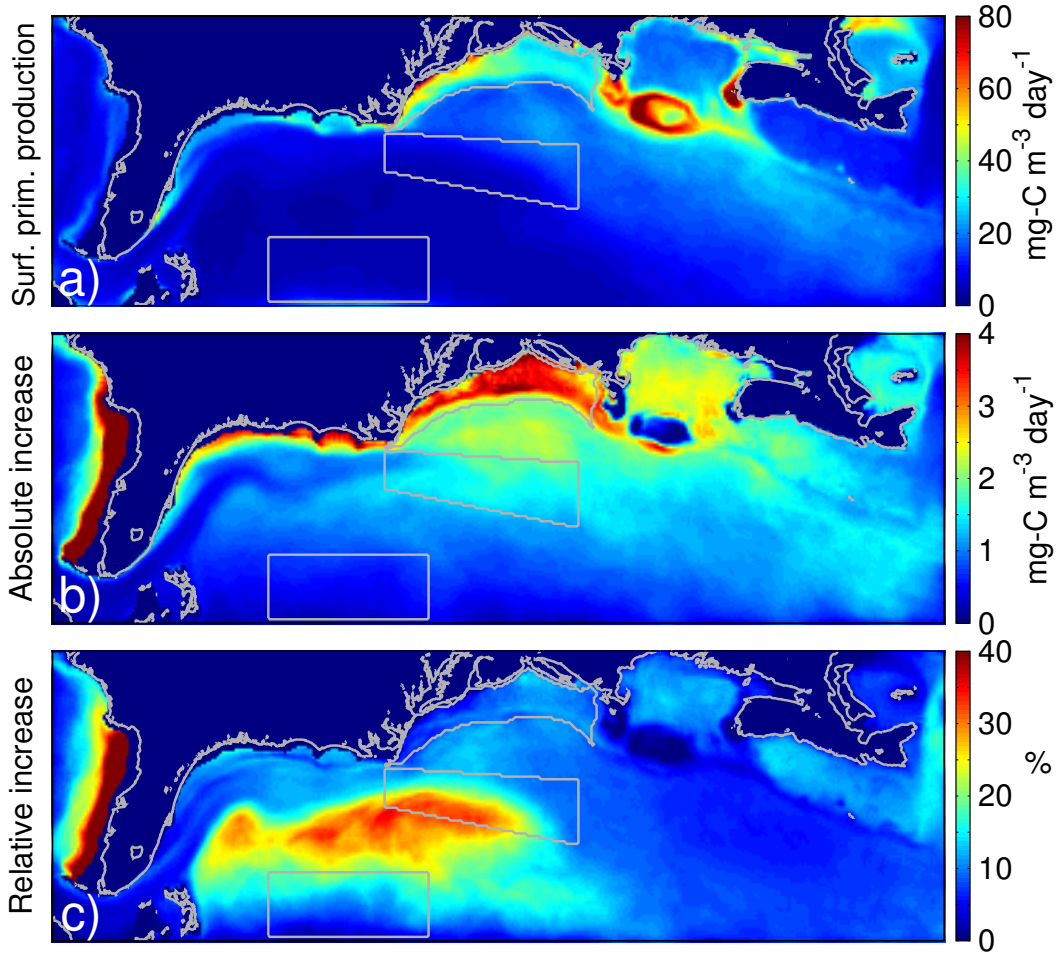

Figure 9. Increase in the primary production of the upper 15 m due to atmospheric nitrogen deposition during the summer (Jul.–Sep. 2004–2008). (a) Primary production from the control (Run 1) averaged over the upper 15 m. The gray polygons represent the regions of interest (see Figure 1). (b) Absolute increase in the primary production of the upper 15 m due to wet+dry deposition (Run 2). (c) Same as b but showing the relative increase (%).

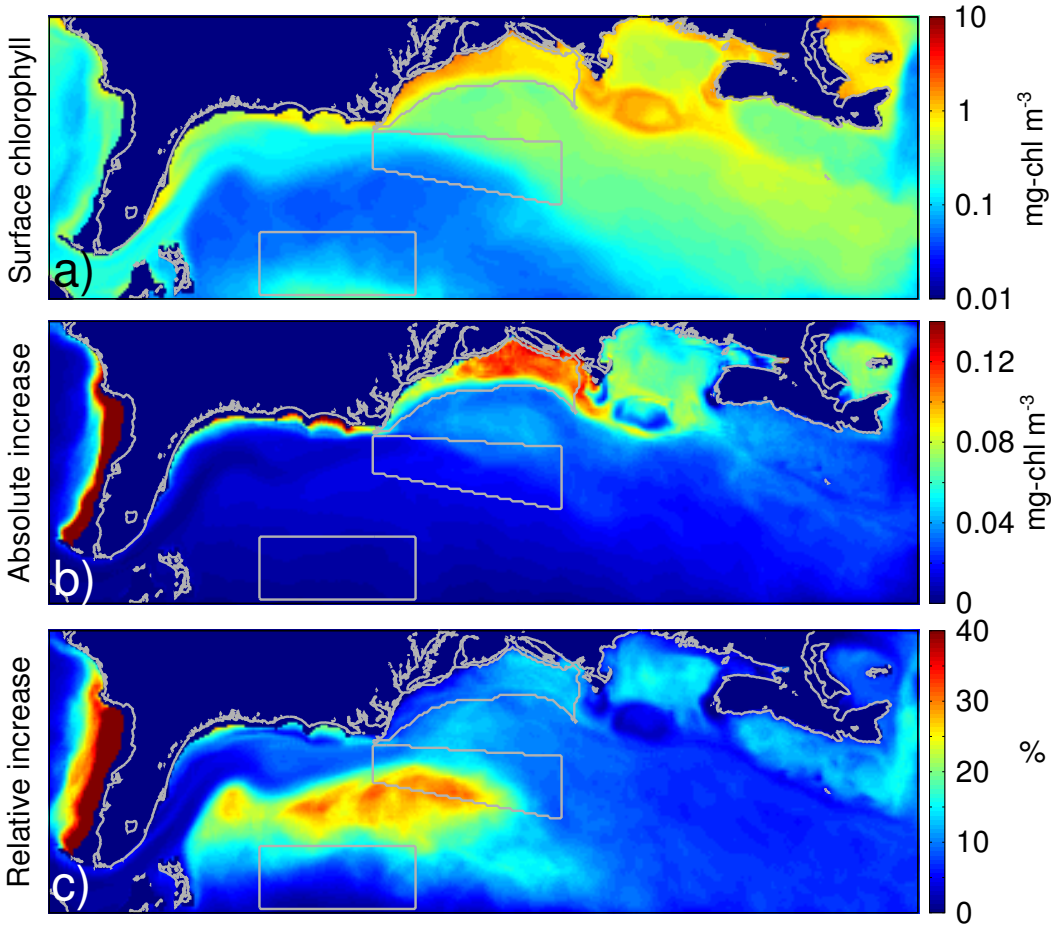

Figure 10. Same as Figure 9 but for chlorophyll averaged over the upper 15 m.

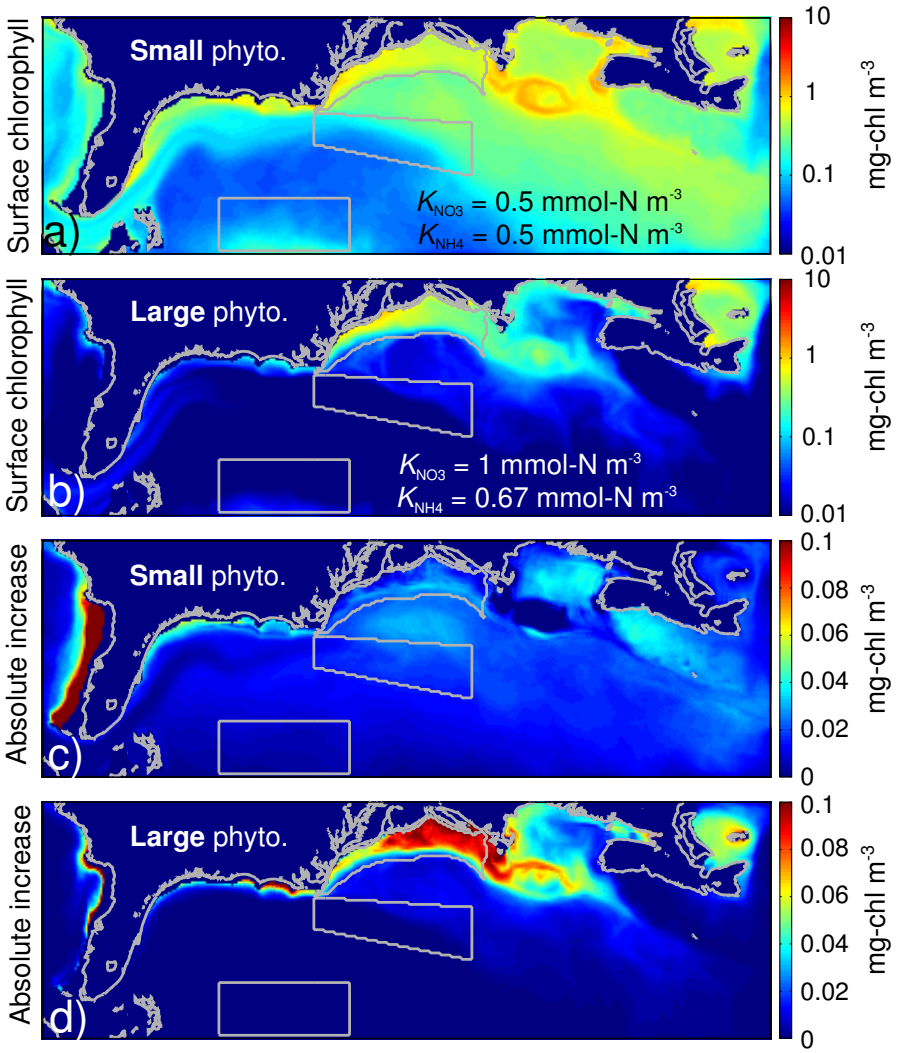

Figure 11. Response to atmospheric deposition for two size classes of phytoplankton. (a) Chlorophyll concentration associated with small phytoplankton (control simulation/Run 1; values averaged over the upper 15 m). (b) Same as a but for large phytoplankton. (c) Absolute increase of small phytoplankton due to wet and dry deposition (Run 2). (d) Same as c but for large phytoplankton. The gray polygons represent the regions of interest (see Figure 1). All fields represent averages over the summer period (Jul.–Sep. 2004–2008).

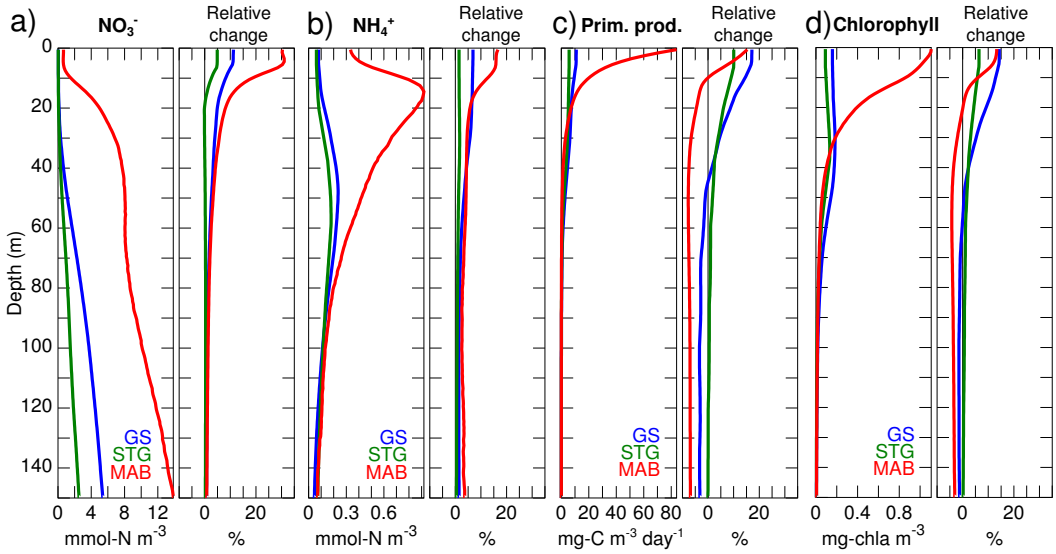

Figure 12. Effects of atmospheric nitrogen deposition below the surface during the summer (average July–Sept. 2004–2008). (a) Horizontally averaged nitrate profile from the control (Run 1) and relative change caused by wet and dry deposition (Run 2). (b, c, and d) Same as 'a' but for ammonium, primary production, and chlorophyll, respectively. MAB is Mid-Atlantic Bight, GS is Gulf Stream and STG is Sub-Tropical Gyre.

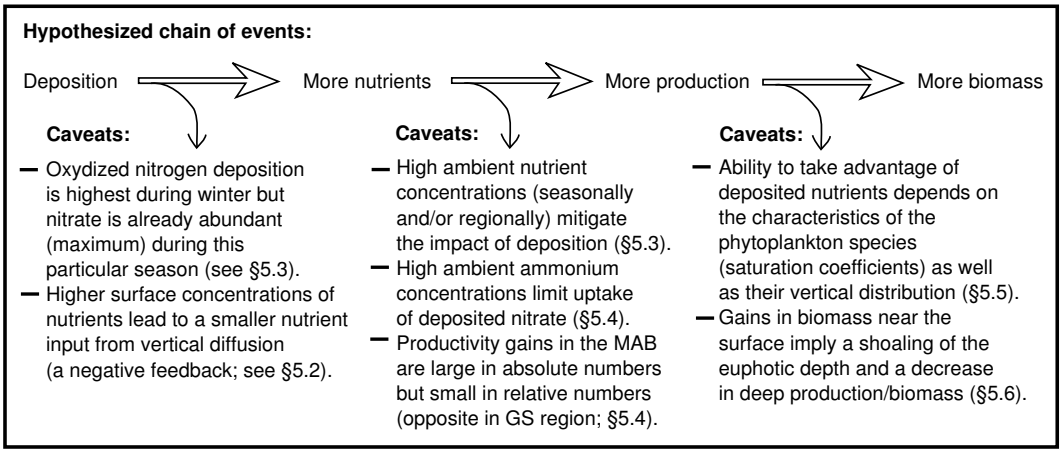

Figure 13. Synthesis of the key results from the study. The schematic compares the hypothesized chain of events and the caveats highlighted by the numerical experiments. MAB is Mid-Atlantic Bight and GS is Gulf Stream.

Table 1. Average nitrate budget (2004–2008) for upper 15 m of the three regions defined in Figure 1[a]

Experiment	Run #	$\partial/\partial t$	H.Adv.[b]	V.Adv.	V.dif.	Biology	Depos.	Res.
			Gulf Stream (GS)					
Control	1	0	−4.68	+2.23	+15.70	−14.12	0	+0.87
Wet+dry	2	0	−4.75	+2.20	+14.96	−14.76	+1.46	+0.89
ΔWet+dry	2 − 1[c]	0	−0.07	−0.03	−0.74	−0.64	+1.46	+0.02
			Sub-Tropical Gyre (STG)					
Control	1	0	−0.05	+0.41	+3.54	−4.75	0	+0.85
Wet+dry	2	0	−0.05	+0.42	+3.28	−5.06	+0.54	+0.87
ΔWet+dry	2 − 1	0	0	+0.01	−0.26	−0.31	+0.54	+0.02
			Mid-Atlantic Bight (MAB)					
Control	1	−0.09	−9.61	+22.58	+16.91	−37.80	0	+7.83
Wet+dry	2	−0.08	−8.90	+23.35	+15.49	−39.22	+1.07	+8.13
ΔWet+dry	2 − 1	+0.01	+0.71	+0.77	−1.42	−1.42	+1.07	+0.30

[a] Units are 10^{-6} mmol-N m^{-2} s^{-1}. See Eq. 8 for the definition of the terms.
[b] Advection is decomposed into horizontal (H.Adv) and vertical components (V.Adv.).
[c] The third row (2 − 1) represents the changes caused by wet and dry nitrogen deposition.

Table 2. Effect of atmospheric nitrogen deposition to surface biogeochemistry during the summer[a]

Experiment	Run # #	sNO3[b] mmol m^{-3}	sNH4 mmol m^{-3}	sDON mmol m^{-3}	sChl mg m^{-3}	sPP^{NO3} mg C m^{-3} d^{-1}	sPP mg C m^{-3} d^{-1}
			Gulf Stream (GS)				
Control	1	0.036	0.077	0.70	0.16	3.1	10.7
ΔWet+Dry	2 − 1[c]	+0.005	+0.0052	+0.08	+0.023	+0.59	+1.90
ΔWet	3 − 1	+0.004	+0.0047	+0.08	+0.019	+0.44	+1.56
ΔDry	2 − 3	+0.001	+0.0005	0	+0.004	+0.15	+0.34
			Sub-Tropical Gyre (STG)				
Control	1	0.029	0.062	0.38	0.086	1.81	5.5
ΔWet+Dry	2 − 1	+0.002	+0.001	+0.04	+0.006	+0.17	+0.58
ΔWet	3 − 1	+0.001	+0.001	+0.04	+0.005	+0.12	+0.45
ΔDry	2 − 3	+0.001	< 0.001	0	+0.001	+0.05	+0.13
			Mid-Atlantic Bight (MAB)				
Control	1	1.0	0.40	1.90	0.78	11.9	33.1
ΔWet+Dry	2 − 1	+0.16	+0.06	+0.11	+0.08	+1.1	+3.1
ΔWet	3 − 1	+0.12	+0.04	+0.11	+0.06	+0.8	+2.4
ΔDry	2 − 3	+0.04	+0.02	0	+0.02	+0.3	+0.7

[a] Values are averaged over the upper 15 m and over Jul.–Sep. 2004–2008 for the regions defined in Figure 1.
[b] Columns are surface nitrate, ammonium, semilabile DON, chlorophyll, nitrate uptake and primary production.
[c] Rows 2 to 4 represent the changes caused by wet and dry nitrogen deposition.

Table 3. Same as Table 2 but averaged between Jan. 1, 2004 and Dec. 31, 2008

Experiment	Run # #	sNO3 mmol m^{-3}	sNH4 mmol m^{-3}	sDON mmol m^{-3}	sChl mg m^{-3}	sPP^{NO3} mg C m^{-3} d^{-1}	sPP mg C m^{-3} d^{-1}
				Gulf Stream (GS)			
Control	1	0.97	0.12	0.53	0.26	9.8	17.4
ΔWet+Dry	2 − 1	+0.024	+0.0056	+0.04	+0.014	+0.44	+1.14
ΔWet	3 − 1	+0.016	+0.0047	+0.04	+0.011	+0.30	+0.86
ΔDry	2 − 3	+0.008	+0.0009	0	+0.003	+0.14	+0.28
				Sub-Tropical Gyre (STG)			
Control	1	0.32	0.088	0.29	0.081	2.63	5.5
ΔWet+Dry	2 − 1	+0.007	+0.002	+0.02	+0.005	+0.16	+0.40
ΔWet	3 − 1	+0.004	+0.002	+0.02	+0.004	+0.11	+0.29
ΔDry	2 − 3	+0.002	< 0.001	0	+0.001	+0.05	+0.11
				Mid-Atlantic Bight (MAB)			
Control	1	3.5	0.41	1.73	0.87	17.8	36.0
ΔWet+Dry	2 − 1	+0.27	+0.03	+0.07	+0.04	+0.6	+1.6
ΔWet	3 − 1	+0.18	+0.02	+0.07	+0.03	+0.4	+1.1
ΔDry	2 − 3	+0.09	+0.01	0	+0.01	+0.2	+0.5